THE JOURNAL OF BIOLOGICAL CHEMISTRY VOL. 291, NO. 41, pp. 21388–21406, October 7, 2016
© 2016 by The American Society for Biochemistry and Molecular Biology, Inc. Published in the U.S.A.

Identification of NEK3 Kinase Threonine 165 as a Novel Regulatory Phosphorylation Site That Modulates Focal Adhesion Remodeling Necessary for Breast Cancer Cell Migration*

Received for publication, March 8, 2016, and in revised form, July 27, 2016 Published, JBC Papers in Press, August 3, 2016, DOI 10.1074/jbc.M116.726190

Katherine M. Harrington[‡1] **and Charles V. Clevenger**[§2]

From the [‡]*Department of Pathology, Robert H. Lurie Comprehensive Cancer Center, Feinberg School of Medicine, Northwestern University, Chicago, Illinois 60611 and the* [§]*Department of Pathology, Virginia Commonwealth University, Richmond, Virginia 23298*

Accumulating evidence supports a role for prolactin (PRL) in the development and progression of human breast cancer. Although PRL is an established chemoattractant for breast cancer cells, the precise molecular mechanisms of how PRL regulates breast cancer cell motility and invasion are not fully understood. PRL activates the serine/threonine kinase NEK3, which was reported to enhance breast cancer cell migration, invasion, and the actin cytoskeletal reorganization necessary for these processes. However, the specific mechanisms of NEK3 activation in response to PRL signaling have not been defined. In this report, a novel PRL-inducible regulatory phosphorylation site within the activation segment of NEK3, threonine 165 (Thr-165), was identified. Phosphorylation at NEK3 Thr-165 was found to be dependent on activation of the extracellular signal-regulated kinase 1/2 (ERK1/2) signaling pathway using both pharmacological inhibition and siRNA-mediated knockdown approaches. Strikingly, inhibition of phosphorylation at NEK3 Thr-165 by expression of a phospho-deficient mutant (NEK3-T165V) resulted in increased focal adhesion size, formation of zyxin-positive focal adhesions, and reorganization of the actin cytoskeleton into stress fibers. Concordantly, NEK3-T165V cells exhibited migratory defects. Together, these data support a modulatory role for phosphorylation at NEK3 Thr-165 in focal adhesion maturation and/or turnover to promote breast cancer cell migration.

The prolactin receptor (PRLR),[3] a member of the cytokine receptor superfamily, is overexpressed in the majority of human breast cancers (1–3). The polypeptide hormone prolactin (PRL) activates its cognate receptor and induces rapid activation of proximal tyrosine kinases, such as Janus kinase 2 (JAK2) and SRC family kinases, leading to transphosphorylation of specific tyrosine residues on the tail of the receptor (4). Distinct docking proteins are recruited to the receptor and provide links to activating various signaling pathways, including signal transducer and activator of transcription (STATs), RAS/MAPK, and phosphatidylinositol 3-kinase (PI3K)/AKT (5–10). PRL/PRLR signaling contributes to the growth, survival, motility, and invasion of human breast cancer cells. PRL has been shown to act as a chemoattractant for breast cancer cells, accompanied by reorganization of the cytoskeleton (11, 12). Furthermore, epidemiological studies indicate that women with high levels of circulating PRL are at an increased risk for developing metastatic breast cancer (13–16). Additionally, knockdown of the long isoform of the PRLR in orthotopic models of breast cancer led to a significant reduction in metastatic spread (17). However, the molecular mechanisms by which PRL/PRLR signaling contributes to the invasive breast cancer cellular phenotype are not fully understood.

NEK3 (never in mitosis gene A related kinase 3) belongs to the NEK family of serine/threonine (Ser/Thr) protein kinases, which is composed of 11 mammalian family members (NEK1–NEK11) (18–20). Compared with other NEK family members, the function of NEK3 remains largely uncharacterized. NEK3 contains a conserved N-terminal catalytic kinase domain (residues 4–257) and two predicted PEST (proline (P)-, glutamic acid (E)-, serine (S)- and threonine (T)-rich) motifs (residues 443–460; 469–495), a domain implicated in regulating both protein stability and protein-protein interactions (21). Previous reports from our laboratory have implicated NEK3 as an important regulator of cell migration. NEK3 is required for the PRL-induced actin cytoskeletal reorganization, which is necessary for directed cell migration to occur. Members of the RHO family of small GTPases, such as RAC, RHO, and CDC42 proteins, are essential regulators of cytoskeleton dynamics (22, 23). Our

* This work was supported in part by National Institutes of Health Grant RO1 CA092265 from NCI (to C. V. C.), the Lynn Sage Cancer Research Foundation (to C. V. C.), and the Avon Foundation (to C. V. C.). The authors declare that they have no conflicts of interest with the contents of this article. The content is solely the responsibility of the authors and does not necessarily represent the official views of the National Institutes of Health.

[1] Supported by a Northwestern University Oncogenesis and Development Training Grant (National Institutes of Health T32 CA080621-08) and by the Malkin Scholars Program from the Robert H. Lurie Comprehensive Cancer Center of Northwestern University.

[2] To whom correspondence should be addressed: Dept. of Pathology, Virginia Commonwealth University, 1101 E. Marshall St., 4-Sanger, P. O. Box 980662, Richmond, VA 23298-0662. Tel.: 804-828-0183; Fax: 804-828-9749; E-mail: charles.clevenger@vcuhealth.org.

[3] The abbreviations used are: PRLR, prolactin receptor; FA, focal adhesion; IP, immunoprecipitation; NEK3, NIMA-related kinase 3; p-, phosphorylated; PRL, prolactin; PPase, phosphatase; PXN, paxillin; WCL, whole cell lysate; GAP, GTPase-activating protein; GEF, guanine nucleotide exchange factor; ANOVA, analysis of variance; EV, empty vector; λ-PPase, λ-protein phosphatase; SC, scrambled; CA, constitutively active; For, forward; Rev, reverse; n.s., not significant.

laboratory previously delineated a signaling pathway linking PRL-stimulated activation of NEK3 to downstream activation of the RHO GTPase RAC1. It is currently thought that NEK3 modulates phosphorylation of the guanine nucleotide exchange factor (GEF) VAV2 and/or phosphorylation of the focal adhesion scaffolding protein paxillin, leading to downstream activation of RAC1 (12, 24). Although the important role of NEK3 in the regulation of PRL-stimulated cell migration has been documented, how NEK3 itself is regulated remains unknown.

PRL/PRLR signaling stimulates the catalytic activity of NEK3; however, the molecular mechanisms of NEK3 activation remain to be elucidated. Many kinases, including the NEK family of protein kinases, are positively regulated by phosphorylation in the activation loop segment. However, regulation of NEK3 activation by phosphorylation has not been examined. In this study, the phosphorylation of NEK3 in response to PRL stimulation and how it contributes to its function in breast cancer cells was investigated. Through site-directed mutagenesis of residues within the activation segment of NEK3, threonine residue 165 (Thr-165) was identified as a major site that regulates the activity and function of NEK3. In addition to being a site of autophosphorylation *in vitro*, phosphorylation of NEK3 Thr-165 was found to be dependent on the activation of the MEK1-ERK1/2 signaling pathway in response to PRL stimulation *in vivo*. Importantly, phosphorylation of NEK3 Thr-165 was found to contribute to its regulation of breast cancer cell migration, focal adhesion remodeling, and actin cytoskeletal rearrangement. These results provide novel mechanistic insight into the role of NEK3 kinase in promoting an invasive breast cancer phenotype.

Results

Identification of NEK3 Autophosphorylation Activity in Vitro—At present, the regulation of NEK3 activation and cellular function is incompletely understood. Autophosphorylation is an important regulatory mechanism for kinase activation, and it generally results in conformational changes necessary for an active kinase. Autophosphorylation of serine/threonine residues within the activation segment of other NEK family members (25–28) has been identified as having a major effect on kinase activation. These observations prompted us to investigate the role of autophosphorylation of activation loop residues as a potentially important regulatory mechanism of NEK3 kinase activation. To begin, *in vitro* translated full-length human wild-type NEK3 containing an N-terminal Myc epitope tag (Myc-WT NEK3) was assessed for its ability to autophosphorylate *in vitro*. Purified Myc-WT NEK3 proteins were incubated in the presence of Mn^{2+} and nonradioactive ATP *in vitro* and analyzed for phosphorylation by Western blotting analysis using α-phosphothreonine (Thr(P)) antibodies. A robust linear time-dependent increase in threonine phosphorylation was detected at the predicted molecular mass of NEK3, ~58 kDa (Fig. 1, *A* and *B*).

To test whether this phosphorylation required the catalytic activity of NEK3, two putative kinase-inactive NEK3 mutants were generated. To this end, key catalytic residues within the kinase domain of NEK3 were mutated by site-directed mutagenesis (D145A and K33R/D127A), which were predicted to render the protein kinase-inactive based upon homology to mouse NEK3 (29, 30) or other human NEK kinases (31, 32). Kinase-inactive NEK3 mutants were then subjected to *in vitro* autophosphorylation assays (Fig. 1*C*). In contrast to wild-type NEK3, phosphorylation was nearly eliminated for both NEK3-D145A and NEK3-K33R/D127A mutants, with reductions of 87.7 and 82.5%, respectively (Fig. 1*D*). Collectively, these data identify NEK3 as a phosphoprotein and suggest that NEK3 is capable of autophosphorylation *in vitro*.

Threonine 165 Is Required for NEK3 Autophosphorylation in Vitro—One of the major mechanisms important in the regulation of protein kinase activation is phosphorylation within the activation segment (defined as the region spanning two highly conserved tripeptide motifs, DEF at the N terminus and APE at the C terminus) (33, 34). Four putative Ser/Thr phosphorylation sites (Ser-148, Ser-153, Thr-161, and Thr-165) were identified within the activation segment of NEK3 (residues 145–172) that could potentially contribute to regulation of its activation. Notably, both the Thr-161 and Thr-165 sites are highly conserved across all vertebrate species examined (Fig. 1*E*). In addition, these sites are conserved in other human NEK family members (Fig. 1*E*), indicating a potentially important regulatory role for these two threonine residues. Therefore, it is not surprising that homologous serine and threonine residues within this region have been shown to be critically important sites of autophosphorylation for other NEK kinases (26, 35). To this end, *in vitro* autophosphorylation assays were utilized to examine the phosphorylation status of these four candidate residues of NEK3 (Ser-148, Ser-153, Thr-161, and Thr-165). Activation segment phospho-deficient mutants were generated by individual mutation of the four candidate Ser/Thr residues within full-length NEK3 to either non-phosphorylatable alanine or valine residues (S148A, S153A, T161V, and T165V) and subjected to *in vitro* autophosphorylation assays (Fig. 1*F*). Two of the mutants (T161V and S148A) displayed moderately reduced autophosphorylation compared with wild-type NEK3, reflected by an approximate 60% reduction in phosphorylated NEK3 on phosphothreonine residues (Fig. 1*G*). Phosphorylation of the S153A mutant was indistinguishable from wild-type NEK3 protein (Fig. 1*G*), indicating that it is unlikely a significant site of NEK3 autophosphorylation *in vitro*. This is in striking contrast to mutation of Thr-165, which was nearly devoid of autophosphorylation and displayed equal phosphorylation levels as the kinase-inactive NEK3 mutant (D145A) used as a control (Fig. 1*G*). Additional NEK3 Thr-165 mutants were created by either substitution with a non-phosphorylatable alanine residue (NEK3-T165A) or to a highly conserved serine residue (NEK3-T165S). Both mutants displayed equivalent levels of autophosphorylation as the NEK3-T165V mutant (data not shown), indicating that the autophosphorylation defects were not specific to mutation to a valine residue. To further investigate the significance of Thr-165 on the enzymatic activity of NEK3, a putative phospho-mimetic mutant was constructed by substitution of the Thr-165 residue with glutamic acid (NEK3-T165E). However, as shown in Fig. 1*F*, NEK3-T165E was unable to rescue NEK3 autophosphorylation activity, and instead displayed equivalent phosphorylation as the phospho-deficient

NEK3-T165V mutant (Fig. 1*G*). This result indicated that substitution at the Thr-165 site with a negatively charged amino acid was unable to compensate for loss of phosphorylation at Thr-165. Importantly, it has been previously shown that mutation to glutamic acid does not routinely function as a phosphorylation mimic and is context-specific (36, 37). Collectively, these results suggest that Thr-165 is essential for the activation of NEK3 and that there is a stringent requirement for a threonine residue at position 165.

These data demonstrated that NEK3 can autophosphorylate on threonine residues *in vitro* and that Thr-165 is a major regulatory site. However, the consequences of NEK3 autophosphorylation remained unclear. To determine the functional consequences of NEK3 autophosphorylation and to assess whether Thr-165 could play a role in NEK3 activation, *in vitro* kinase assays were performed with *in vitro* translated NEK3 (wild-type and phospho-mutants), and NEK3 activation was measured by monitoring substrate phosphorylation by West-

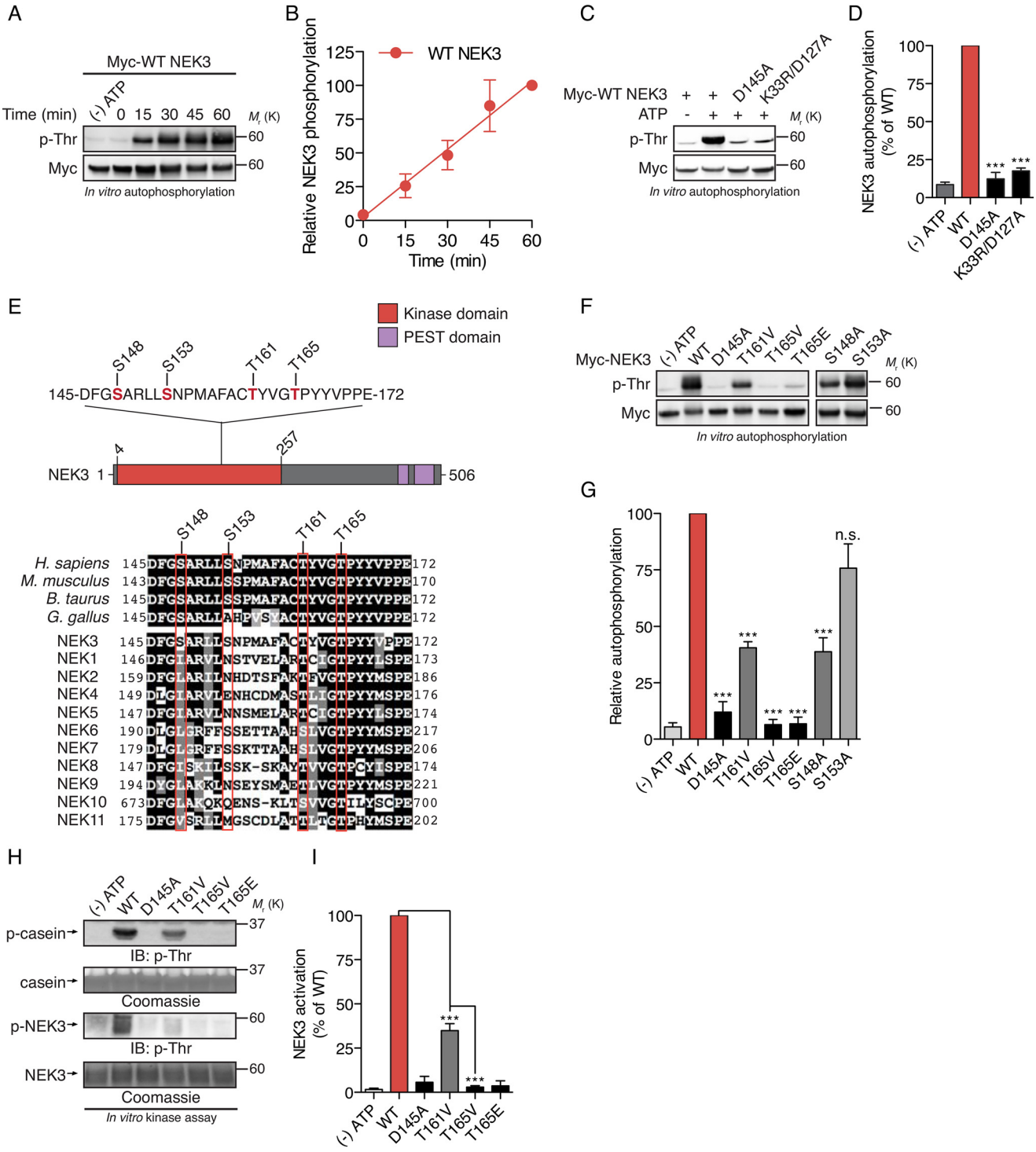

ern blotting. As there are presently no endogenous NEK3 direct substrates reported in the literature, dephosphorylated casein was used as an exogenous substrate in the reaction. Casein had been previously reported as a suitable substrate for NEK3, as well as other NEK family members (24, 25). In agreement, wild-type NEK3 showed robust activity toward phosphorylating casein, although, as expected, kinase-inactive NEK3 (NEK3-D145A) was unable to phosphorylate casein *in vitro*. Mutation of the Thr-161 site (T161V) resulted in a loss of 65% of kinase activity. Autophosphorylation at Thr-165 appears to be absolutely critical for the activity of NEK3, as mutation of this site Thr-165 (T165V and T165E) resulted in a loss of 97% of kinase activity with respect to its ability to phosphorylate casein as an exogenous substrate, equivalent to kinase-inactive NEK3 (Fig. 1, *H* and *I*). These results demonstrated that NEK3 autophosphorylation correlates with its activity and suggests that NEK3 requires Thr-165, and to a lesser extent Thr-161, for its activation.

Development of a Novel Antibody That Recognizes NEK3 Thr-165 Phosphorylation—These data implicated Thr-165 as a major regulatory site within the activation segment of NEK3 and was therefore chosen for further detailed study. However, it was uncertain whether this residue could be playing a structural role necessary for NEK3 activation or whether it could be catalytically involved in the autophosphorylation of an alternative residue without becoming phosphorylated itself. Indeed, NEK3 Thr-165 is located within the highly conserved GT motif within the P + 1 loop of the predicted activation segment of NEK3, a region previously shown to be structurally important for kinase activation (34). Therefore, to address whether Thr-165 itself was a target for autophosphorylation, a novel rabbit polyclonal antibody was generated against a peptide comprised of residues 160–170 of human NEK3 (^{160}CTYVG(pT)PYYVP^{170}) containing the phosphorylated Thr-165 residue (p-NEK3 (T165); see under "Experimental Procedures").

First, the specificity of this antibody to detect NEK3 phosphorylated at Thr-165 was evaluated. To confirm that the signal detected by the p-NEK3 (T165) antibody was specific to the phosphorylated form of NEK3, autophosphorylated reaction products of Myc-WT NEK3 were treated with λ-protein phosphatase (λ-PPase) to globally remove phosphate groups. As shown in Fig. 2*A*, the p-NEK3 (T165) antibody detected robust phosphorylation at NEK3 Thr-165 when allowed to autophosphorylate in the presence of nonradioactive ATP (Fig. 2*A*, *2nd lane*). Treatment with λ-phosphatase completely inhibited detection of NEK3 phosphorylated at Thr-165 (Fig. 2*A*, *lane 4*), whereas total NEK3 protein levels (as detected by the anti-Myc antibody) remained unchanged. As a control, parallel blots were incubated with anti-phosphothreonine antibodies to confirm that λ-phosphatase treatment removed all phosphorylated threonine residues (Fig. 2*A*). Quantification of these results showed that λ-phosphatase treatment removed 97% of the antibody signal (Fig. 2*B*), suggesting that the p-NEK3 (T165) antibody is highly specific for phosphorylated residues. To further assess the specificity of the p-NEK3 (T165) antibody, peptide competition studies were performed. The signal detected by the p-NEK3 (T165) antibody on autophosphorylated reaction products was completely inhibited by the immunizing phosphopeptide (*NEK3 pT165*; ^{161}TYVG(pT)PYYVP^{170}), but not with equal

FIGURE 1. **Autophosphorylation at Thr-165 is required for NEK3 kinase activity *in vitro*.** *A* and *B,* immunoblot analysis (*A*) and quantification (*B*) of the time-dependent increase in threonine phosphorylation of wild-type NEK3 *in vitro*. Full-length wild-type NEK3 containing a C-terminal Myc affinity tag (Myc-WT NEK3) was translated *in vitro* and subjected to *in vitro* autophosphorylation assays in the presence of nonradioactive ATP for the indicated time points. NEK3 protein phosphorylation was detected by Western blotting analysis with α-phosphothreonine antibodies (*p-Thr*); the Western blot with α-Myc antibodies showed equal expression of NEK3 protein. NEK3 phosphorylation was quantified by densitometric analysis of the phosphothreonine signal normalized to the total NEK3 protein levels (detected by the α-Myc antibody) and was plotted over the incubation times of the autophosphorylation reaction; each time point is graphed as the mean ± S.E. of three independent experiments. Data are presented relative to the 60-min time point, which is set as 100%. The *solid line* shows the linear fit of the data ($R^2 = 0.8393$). Western blots are representative of three independent experiments. *C* and *D,* NEK3 autophosphorylation requires an intact kinase domain. Wild-type Myc-NEK3 (WT) or kinase-inactive NEK3 mutants (D145A, K33R/D127A) were *in vitro* translated and purified by immunoprecipitation with α-Myc antibodies. *In vitro* autophosphorylation assays were performed for 45 min and analyzed by Western blotting analysis with α-phosphothreonine antibodies; Western blotting analysis with α-Myc antibodies showed equal protein expression of NEK3 constructs. NEK3 autophosphorylation was quantified by densitometric analysis of the phosphothreonine signal normalized to the total NEK3 protein levels (detected by the α-Myc antibody) and presented as the mean ± S.E. of three independent experiments. Data are presented relative to WT NEK3, which is set as 100%. ***, $p \leq 0.001$ compared with WT NEK3; ANOVA was followed by Bonferroni's multiple comparison test. Western blots are representative of three independent experiments. *E,* schematic representation of the predicted domain structures of human NEK3 protein. NEK3 is composed of a kinase domain (residues 4–257) and two predicted PEST motifs (residues 443–460; 469–495). Potential serine/threonine (Ser/Thr) sites of autophosphorylation within the activation segment (residues 145–172) are highlighted in *red* (Ser-148, Ser-153A, Thr-161, and Thr-165). The amino acid sequence of the activation segment of NEK3 was aligned among species (*top*) and aligned with the 11 human NEK kinase family members (*bottom*). Sequences were aligned using T-Coffee and displayed with Boxshade. Amino acids shaded in *black* indicate complete conservation; *gray* indicates conservation of similar amino acids; and *dash* indicates a missing amino acid. *F,* NEK3 Thr-165 is required for autophosphorylation activity *in vitro*. Purified *in vitro* translated Myc-NEK3 wild-type (*WT*), kinase-inactive NEK3 (D145A), or indicated NEK3 activation loop mutants (T161V, T165V, T165E, S148A, and S153A) were used to perform *in vitro* autophosphorylation assays for 45 min in the presence of nonradioactive ATP. NEK3 protein phosphorylation was determined by immunoblotting with α-phosphothreonine antibodies (*p-Thr*); Western blotting analysis with α-Myc antibodies showed equal protein expression of NEK3 constructs. Western blots are representative of three (*left panel*) or four (*right panel*) independent experiments. *G,* quantification of the autophosphorylation level of the indicated NEK3 mutants relative to wild-type NEK3 (WT) presented as the mean ± S.E. of three (D145A, T161V, T165V, and T165E) or four (S148A and S153A) independent experiments; Western blot images for NEK3 threonine mutants (*left panel*) and serine mutants (*right panel*) represent independent membranes (delineated by *black outlines*) where mutant autophosphorylation activity was calculated relative to an internal WT NEK3 control. ***, $p \leq 0.001$, *n.s.*, $p > 0.05$ compared with WT NEK3 (indicated in figure); T161V *versus* T165V, $p \leq 0.001$; D145A *versus* T165V, *n.s.,* T165V *versus* T165E, *n.s.*; ANOVA was followed by Bonferroni's multiple comparison test. *H,* NEK3 Thr-165 is required for kinase activation. An *in vitro* kinase assay was performed using purified Myc-NEK3 wild-type (*WT*), kinase-inactive NEK3 (D145A) or NEK3 threonine phospho-mutants (T161V, T165V, and T165E) in the presence of nonradioactive ATP with dephosphorylated casein as a substrate for the reaction. Autophosphorylation of NEK3 and trans-phosphorylation of casein were detected by immunoblotting with α-phosphothreonine antibodies (*p-Thr*). A parallel gel was stained with Coomassie to determine that an equal amount of casein and NEK3 was present in each reaction. Western blots are representative of three independent experiments. *I,* NEK3 kinase activity was quantified by densitometric analysis of the phosphothreonine casein signal normalized to the total amount of casein in each reaction and presented as the mean ± S.E. of three independent experiments. Data are presented relative to WT NEK3, which is set as 100%. WT *versus* D145A, $p \leq 0.001$; WT *versus* T161V, $p \leq 0.001$ (indicated in figure); WT *versus* T165V, $p \leq 0.001$; T161V *versus* T165V, $p \leq 0.001$ (indicated in figure); D145A *versus* T165V, n.s; T165V *versus* T165E, n.s.; ***, $p \leq 0.001$, n.s. $p > 0.05$; ANOVA was followed by Bonferroni's multiple comparison test.

amounts of the corresponding non-phosphorylated peptide (*NEK3 T165 NP*; ^{161}TYVGTPYYVP^{170}) (Fig. 2, *C* and *D*). Given the proximity of the Thr-165 site to Thr-161, the p-NEK3 (T165) antibody was evaluated to determine whether it would cross-react with this nearby site. Pre-incubation with a phosphorylated peptide to the Thr-161 site (*NEK3 pT161*; ^{158}FAC(pT)YVGTPY^{167}), resulted in no change in the signal detected by the p-NEK3 (T165) antibody (Fig. 2, *C* and *D*). Taken together, these results indicate that the rabbit polyclonal p-NEK3 (T165) antibody specifically recognizes NEK3 when phosphorylated at residue Thr-165.

NEK3 Is Phosphorylated at Residue Thr-165 within Its Activation Segment—To ascertain whether Thr-165 was indeed a site of NEK3 autophosphorylation, the reaction product from autophosphorylated wild-type NEK3 and kinase-inactive NEK3 mutants (D145A and K33R/D127A) was analyzed by Western blotting using the p-NEK3 (T165) antibody. Importantly, these experiments revealed that NEK3 autophosphorylation at Thr-165 was markedly inhibited for both kinase-inactive NEK3 mutants (Fig. 2, *E* and *F*), indicating that phosphorylation at the Thr-165 site is strictly dependent on the kinase activity of NEK3 *in vitro*. To explore the possibility that phosphorylation at Thr-165 was dependent on the Thr-161 site, the NEK3-T161V mutant was assessed for its ability to autophosphorylate at Thr-165. As shown in Fig. 2*G*, NEK3-T161V retained phosphorylation at Thr-165; however, it was reduced by 52.0% compared with wild-type NEK3 (Fig. 2*H*). These results suggest that the Thr-161 site is not required for autophosphorylation to occur at Thr-165, but it may play a modulatory role. As expected, the T165V mutant used as a control showed no significant phosphorylation detected by the p-NEK3 (T165) antibody. Collectively, these results demon-

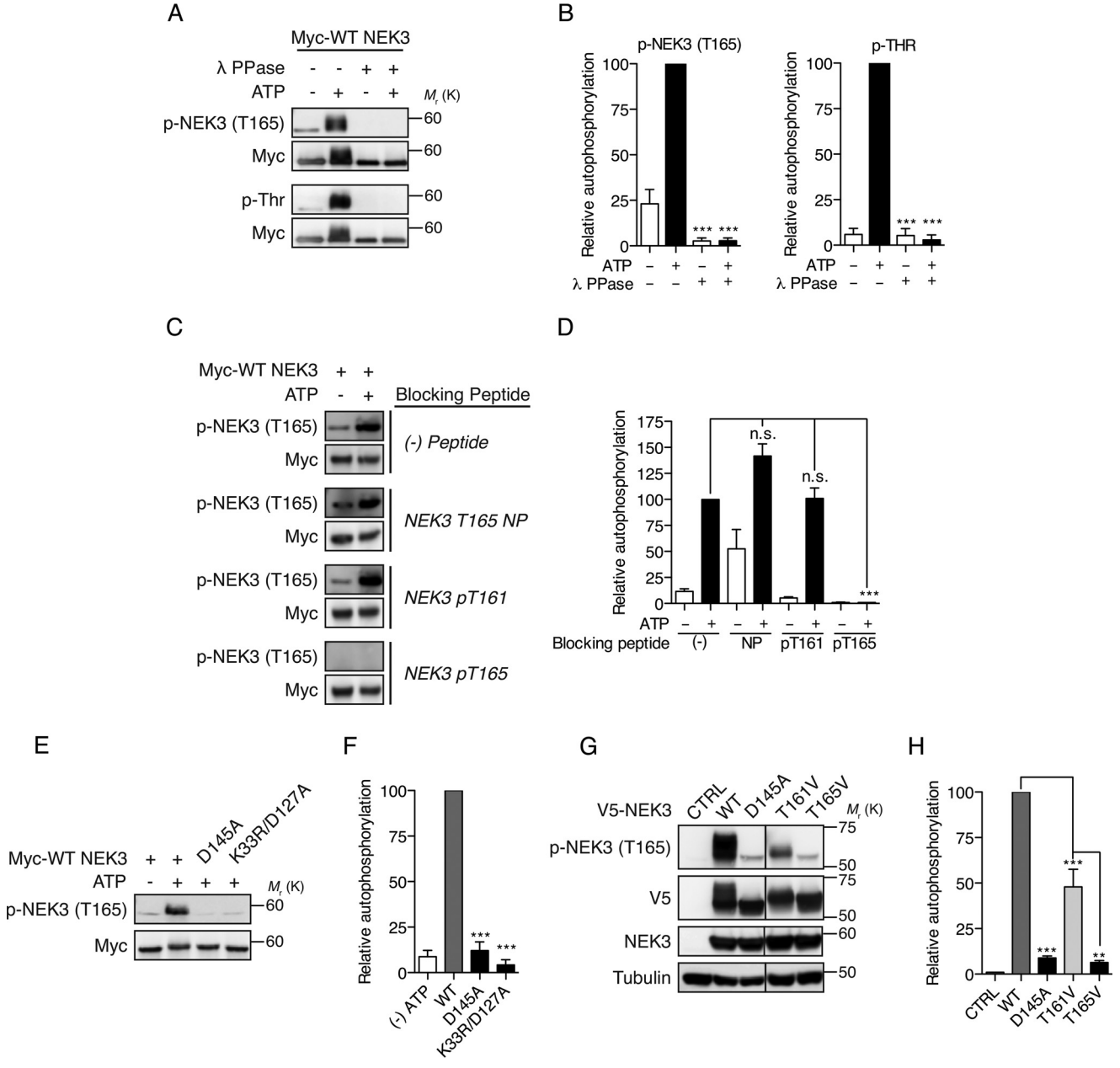

strate a key role for Thr-165 regulating NEK3 autophosphorylation *in vitro*.

Activation of the ERK1/2 Pathway Regulates Phosphorylation of NEK3 Thr-165—To gain insight into the molecular mechanisms regulating NEK3 activation *in vivo*, the contribution of PRL-stimulated phosphorylation of NEK3 at Thr-165 was examined. Collectively, the above data demonstrated that NEK3 Thr-165 is a major autophosphorylation site *in vitro*. However, it was unclear whether phosphorylation at residue Thr-165 was dependent on the catalytic activity of NEK3 *in vivo*. To this end, NEK3 phosphorylation at Thr-165 was examined directly by Western blotting analysis following PRL stimulation of MCF-7 cells expressing wild-type NEK3 protein (V5-WT NEK3) or kinase-inactive NEK3 protein (V5-NEK3-D145A). Upon PRL stimulation, phosphorylation at Thr-165 NEK3 was increased to relatively equivalent levels for both wild-type and kinase-inactive NEK3 proteins (Fig. 3, *A* and *B*). Surprisingly, these data demonstrate that the catalytic activity of NEK3 is not required for phosphorylation at Thr-165 in response to PRL stimulation *in vivo* and suggest that mechanisms other than autophosphorylation may additionally contribute to activation *in vivo*.

Thus, this finding suggested that phosphorylation of NEK3 at Thr-165 may be mediated by an upstream kinase *in vivo*. To identify potential upstream kinase(s), a non-biased bioinformatics approach was employed using the kinase prediction software, Scansite 2.0 (38). Extracellular signal-regulated protein kinase-1 and -2 (ERK1/2) were identified as likely candidates that could target NEK3 Thr-165. ERK1/2 generally phosphorylate Ser/Thr residues that lie within the Xaa-(Ser/Thr)-Pro (*X*(S/T)P) consensus motif (39). Importantly, the residues surrounding the NEK3 Thr-165 site (^{164}G**T**P^{166}) fall within this ERK1/2 consensus motif. Activation of ERK1/2 occurs through dual-phosphorylation of threonine and tyrosine residues by mitogen-activated protein kinase (MAPK) kinase (MEK1/2 (40)) (ERK1, Thr-202/Tyr-187; ERK2, Thr-185/Tyr-187). To begin to investigate the possible contribution of ERK1/2-mediated signaling on NEK3 phosphorylation at Thr-165, MCF-7 cells stably expressing wild-type NEK3 protein (V5-WT NEK3) or kinase-inactive NEK3 protein (V5-NEK3-D145A) were pre-treated with the MEK inhibitor, U0126, to inhibit ERK activation in response to PRL stimulation. Western blotting analysis revealed a dramatic decrease in the phosphorylation at NEK3 Thr-165 in both wild-type and kinase-inactive NEK3 cells (Fig. 3*C*).

To further explore whether ERK1/2 could be responsible for mediating phosphorylation at NEK3 Thr-165, NEK3 was assayed for its ability to physically associate with ERK1/2 *in vivo* by co-immunoprecipitation experiments in HEK293T cells. Immunoprecipitation of exogenous V5-WT NEK3 with anti-V5 antibodies demonstrated that endogenous ERK1/2 readily associated with NEK3 (Fig. 3*D*, *2nd lane*), whereas minimal interaction was detected using an isotype control antibody (Fig. 3*D*, *1st lane*). Quantification revealed an 8-fold increase in the association of ERK1/2 with NEK3 compared with the IgG negative control (Fig. 3*E*). These data identified a novel, specific interaction between NEK3 and ERK1/2 *in vivo*.

To substantiate these findings, a constitutively active form of MEK1 (CA-MEK1) was expressed in HEK293T cells to activate endogenous ERK1/2. Co-expression of CA-MEK1 led to a prominent increase in phosphorylation at NEK3 Thr-165 (Fig. 3, *F* and *G*). Treatment of the NEK3 immunocomplexes with λ-protein phosphatase abolished the MEK1-induced phosphorylation at NEK3 Thr-165, which confirmed that the observed increase in signal detected with the phospho-specific antibody was the consequence of phosphorylation (Fig. 3, *F* and *G*). Activation of the MEK1-ERK1/2 pathway was confirmed by increased phosphorylation of ERK1/2 at Thr-202/Tyr-204 (Fig. 3*F*). Furthermore, CA-MEK1 was also capable of inducing phosphorylation at Thr-165 of kinase-inactive NEK3 (D145A), which indicated that the phosphorylation observed was due to the MEK1-ERK1/2 pathway and was independent of the cata-

FIGURE 2. **Identification of Thr-165 as a novel NEK3 autophosphorylation site *in vitro*.** *A* and *B,* p-NEK3 (T165) antibody is phosphospecific. *In vitro* translated Myc-WT NEK3 was immunopurified, and an *in vitro* autophosphorylation assay was performed in the presence or absence of nonradioactive ATP. Subsequently, immunoprecipitates were subjected to λ-PPase treatment and separated by SDS-PAGE, and phosphorylation was detected by immunoblotting with α-p-NEK3 (T165) antibodies (*top*) or α-phosphothreonine antibodies (*bottom*). *Graphs* show relative densitometric quantification of Western blot band intensities for the ratio of p-NEK3 (T165) (*left panel*) and total NEK3 threonine phosphorylation (*right panel*) normalized to total NEK3 protein levels detected with the α-Myc antibody. ***, $p \leq 0.001$; ANOVA was followed by Bonferroni's multiple comparison test. Western blots are representative of two independent experiments. *C* and *D,* Western blotting analysis of Myc-WT NEK3 autophosphorylation reactions using the p-NEK3 (T165) antibody in the presence of peptide competition. The p-NEK3 (T165) antibody was pre-blocked by incubation with 4 μg/ml of the following peptides for 30 min at 4 °C: *NEK3 T165 NP*, TYVGTPYYVP; *NEK3 pT161*, FAC(pT)YVGTPY; *NEK3 pT165*, TYVG(pT)PYYVP, and incubation without peptide was used as a control. (*pT*) indicates the phosphorylated residue; *NP*, indicates non-phosphorylated; *graphs* show relative densitometric quantification of Western blot band intensities for the ratio of p-NEK3 (T165) normalized to total NEK3 levels detected with the α-Myc antibody. Values are presented relative to the no peptide control, which is set as 100%. ***, $p \leq 0.001$; *n.s.*, $p > 0.05$ compared with the no peptide control; ANOVA was followed by Bonferroni's multiple comparison test. Western blots are representative of three independent experiments. *E* and *F,* phosphorylation of NEK3 Thr-165 is dependent on its catalytic activity *in vitro*. Wild-type Myc-NEK3 (WT) or kinase-inactive NEK3 mutants (D145A, K33R/D127A) were *in vitro* translated and purified by immunoprecipitation with α-Myc antibodies. *In vitro* autophosphorylation assays were performed for 45 min, and NEK3 phosphorylation was analyzed by Western blot using α-p-NEK3 (T165) antibodies. Immunoblotting with α-Myc antibodies showed similar protein levels of the NEK3 constructs. NEK3 autophosphorylation was quantified by densitometric analysis of the p-NEK3 (T165) signal normalized to the total NEK3 protein levels (detected by the α-Myc antibody) and presented as the mean ± S.E. of three independent experiments. Data are presented relative to WT NEK3, which is set as 100%. ***, $p \leq 0.001$ compared with WT NEK3; ANOVA was followed by Bonferroni's multiple comparison test. Western blots are representative of three independent experiments. *G* and *H,* NEK3 autophosphorylation at Thr-165 *in vitro* is dependent on Thr-161. An *in vitro* autophosphorylation assay (45 min) was performed using V5-NEK3 (wild-type and mutants) immunoprecipitates from stable MCF-7 cells. NEK3 protein phosphorylation was analyzed by Western blot using α-pT165-NEK3 antibodies; equal protein levels of immunoprecipitates were confirmed by blotting with α-V5 antibodies. Whole cell lysates (*WCL*) were probed with α-NEK3 antibodies to confirm equal expression of NEK3 constructs; tubulin was used as a loading control. The *black line* indicates non-adjacent lanes on the same gel. The *graph* shows quantification of NEK3 autophosphorylation of the NEK3 threonine phospho-mutants relative to wild-type NEK3 presented as the mean ± S.E. of three independent experiments; differences between groups were determined by one-way ANOVA was followed by Bonferroni's multiple comparison test; WT *versus* D145A, $p \leq 0.001$; WT *versus* T161V, $p \leq 0.001$ (indicated in figure); WT *versus* T165V, $p \leq 0.001$; T161V *versus* T165V, $p \leq 0.01$ (indicated in figure); D145A *versus* T165V, *n.s.*, ***, $p < 0.001$; **, $p < 0.01$; *n.s*, $p > 0.05$. Western blots are representative of three independent experiments.

lytic activity of NEK3 (Fig. 3, *H* and *I*). Taking into account that ERK1/2 are the only described substrates of MEK1 to date (41, 42), these results implicate activation of the ERK1/2 pathway as being necessary for phosphorylation of Thr-165 within the activation segment of NEK3 *in vivo*.

Prolactin is a known activator of the MEK1-ERK1/2 pathway (7–9, 43–45). Therefore, it was examined whether the activation of ERK1/2 in response to PRL stimulation influenced phosphorylation of endogenous NEK3 at Thr-165. Quiescent T-47D breast cancer cells were stimulated with PRL for various time points, and phosphorylation of endogenous NEK3 at Thr-165 was examined by Western blotting analysis using p-NEK3 (T165) antibodies (Fig. 4*A*). Phosphorylation at NEK3 Thr-165 was minimally detected in quiescent T-47D cells, but it significantly increased following PRL treatment (Fig. 4, *A* and *B*) with peak phosphorylation occurring at 15–30 min of PRL treatment. Pre-treatment of cells with U0126 to inhibit the PRL-induced activation of MEK1-ERK1/2 signaling resulted in a marked decrease in phosphorylation at NEK3 Thr-165, and when quantified it was revealed to be ~70% reduced (Fig. 4*B*). Similar results were obtained with MCF-7 cells, indicating that these observations are not restricted to a single cell line (Fig. 4, *C* and *D*). Notably, phosphorylation at NEK3 Thr-165 correlates with the activation of ERK1/2 observed in response to PRL stimulation (Fig. 4, *A* and *C*).

Importantly, it has been previously reported that U0126 can also inhibit the MEK5-ERK5 signaling pathway (46, 47), which can also be activated in response to PRL in breast cancer cell lines (48). Therefore, to further validate these findings, T-47D cells stably expressing V5-WT NEK3 were transfected with small interfering RNA (siRNA) to specifically silence gene expression of ERK1/2 or a non-targeting control siRNA. The effectiveness of siRNA-mediated gene silencing of ERK1/2 was confirmed by Western blotting analysis and was found to be ~60% reduced (Fig. 4, *E* and *F*). Reduction of ERK1/2 expression resulted in a marked inhibition of NEK3 phosphorylation

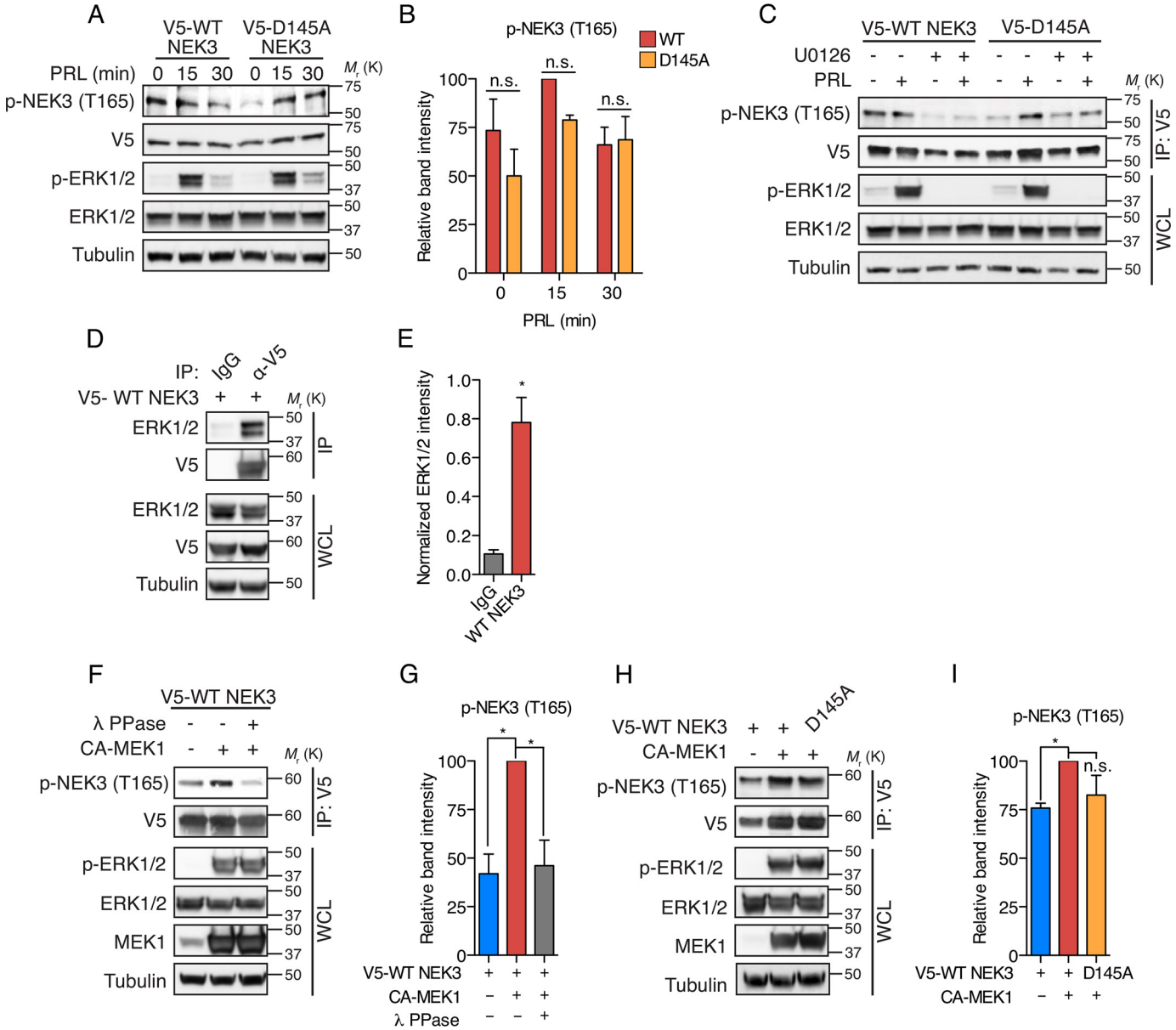

at Thr-165 in response to PRL stimulation (Fig. 4, *E* and *F*). Taken together, these results strongly suggest that the activation of the ERK1/2 pathway in response to PRL stimulation is responsible for phosphorylation of NEK3 at Thr-165 *in vivo*.

Phosphorylation at NEK3 Thr-165 Leads to Altered Focal Adhesion Morphology and Regulates Cell Motility—We next sought to determine the biological significance of phosphorylation at NEK3 Thr-165. It was previously reported that NEK3 contributes to cell migration and invasion of breast cancer cells *in vitro* (12); however, the molecular mechanisms remain to be elucidated. Cell migration and invasion are critical biological processes that are the first necessary steps in the metastatic cascade. In order for efficient cell migration to occur, the assembly and disassembly of focal adhesions must be tightly regulated. Given that NEK3 had been previously shown to interact with the focal adhesion adaptor protein, paxillin (12), it was hypothesized that NEK3 may be regulating cell migration and invasion, at least in part, through control of focal adhesion dynamics. Importantly, previous published reports demonstrated a key role for ERK1/2 in the regulation of focal adhesion maturation and turnover (49, 50). Thus, it was determined what effect pharmacological inhibition of ERK1/2 activation by the MEK inhibitor, U0126, had on focal adhesion morphology. MCF-7 cells stably expressing V5-WT NEK3 were pre-treated with U0126, stimulated with PRL, and immunostained for PXN phosphorylated at tyrosine 118 (p-PXN) to visualize the focal adhesion complex (Fig. 5*A*). Quantification of FA morphology indicated that U0126 treatment resulted in a significant increase in the average area of individual focal adhesions (Fig. 5*B*). In addition, the percentage of cell area covered by focal adhesion complexes was significantly increased by U0126 treatment compared with cells treated with DMSO vehicle control (Fig. 5*C*). This increase could be attributed to *de novo* formation of focal adhesions; however, the number of focal adhesions normalized to cell area was found to be relatively equivalent between vehicle-treated and U0126-treated cells (data not shown). Therefore, these data suggest that inhibition of ERK1/2 signaling may regulate focal adhesion morphology by promoting maturation of existing focal adhesion complexes and/or inhibiting focal adhesion disassembly, which is in concordance with previously published reports (50–52). We therefore hypothesized that ERK1/2-mediated phosphorylation at NEK3 Thr-165 may be required for its role in regulating the focal adhesion complex.

To this end, endogenous *NEK3* was depleted from MCF-7 cells by retroviral infection of a short hairpin RNA (shRNA) vector targeted to the cDNA of *NEK3*, which resulted in a marked decrease in NEK3 expression as determined by Western blotting analysis (Fig. 5, *D* and *E*). Following PRL stimulation, stable MCF-7 knockdown cells were fixed and stained for PXN phosphorylated at tyrosine 118 (p-PXN), to mark the focal adhesion complex. Cells with silenced NEK3 expression exhibited altered focal adhesion morphology, with focal adhesions that appeared significantly longer (Fig. 5*F*). Quantification of focal adhesions revealed that there was a 70% increase in the average FA size, as well as a 4-fold increase in the percentage of cell area occupied by focal adhesions in the shNEK3 cells compared with control cells (Fig. 5, *G* and *H*). Importantly, no differences in p-PXN or total PXN protein levels between MCF-7 cells expressing shNEK3 and empty vector or scrambled control cells were detected by Western blotting analysis (data not shown).

Small adhesion structures, known as focal complexes, can either rapidly turn over or mature into larger long-lived focal adhesions. Continuous turnover/disassembly of focal adhesions is critical for rapid cell migration to occur, and it has been shown that large stable focal adhesions tend to inhibit cell migration (53). Importantly, depletion of NEK3 significantly reduced cell migration of MCF-7 breast cancer cells (Fig. 5, *I*

FIGURE 3. **MEK1/2-ERK1/2 signaling promotes NEK3 Thr-165 phosphorylation *in vivo*.** *A* and *B,* PRL stimulates phosphorylation of kinase-inactive NEK3 at Thr-165 in breast cancer cells *in vivo*. Serum-starved MCF-7 cells stably expressing wild-type NEK3 (*WT*) or kinase-inactive NEK3 (D145A) were stimulated with PRL (250 ng/ml) for the indicated times and subjected to immunoblot analysis using α-p-NEK3 (T165) antibodies; α-V5 antibodies detected total NEK3 expression levels. Detection of phosphorylated ERK1/2 with α-p-ERK1/2 (T202/Y204) antibodies showed relatively equivalent activation of PRL-induced downstream signaling. Tubulin was used as a protein loading control. The *graph* shows the relative densitometric quantification of Western blot band intensities for the ratio of p-NEK3 (T165) normalized to total NEK3 levels detected with the α-V5 antibody. No significant difference in phosphorylation at NEK3 Thr-165 between WT and kinase-inactive NEK3 was found, *n.s.*, $p > 0.05$; two-way ANOVA was followed by Bonferroni's multiple comparison test. Western blot images are representative of three independent experiments. *C*, pharmacological inhibition of MEK1/2-ERK1/2 signaling inhibits phosphorylation at p-NEK3 (T165). Serum-starved MCF-7 cells stably expressing wild-type NEK3 (WT) or kinase-inactive NEK3 (D145A) were left untreated or were pre-treated with the MEK inhibitor, U0126, for 2 h. Cells were stimulated with PRL (250 ng/ml) for 15 min and V5-NEK3 proteins were isolated from whole cell lysates by immunoprecipitation. Immunocomplexes were probed with α-p-NEK3 (T165) antibodies; α-V5 antibodies detected total NEK3 expression levels. Detection of phosphorylated ERK1/2 with α-p-ERK1/2 (T202/Y204) antibodies showed inhibition of the compound's target. Tubulin was used as a protein loading control. A representative Western blot is shown. *D* and *E,* exogenous NEK3 associates with endogenous ERK1/2. Cell lysates from HEK293T cells expressing wild-type V5-NEK3 were immunoprecipitated (*IP*) with α-V5 antibodies (or IgG isotype control antibodies), followed by immunoblotting with antibodies against total ERK1/2 (to detect binding of endogenous ERK1/2) or anti-V5 (to confirm immunoprecipitation of NEK3). The *graph* shows the densitometric quantification of the band intensity of ERK1/2 co-immunoprecipitated with WT NEK3 (or IgG negative control) normalized to the input levels of ERK1/2 present in the whole cell lysate; *, $p \leq 0.05$; Student's *t* test. Western blot images are representative of three independent experiments. *F* and *G,* CA-MEK1 increases NEK3 Thr-165 phosphorylation. Cell lysates were prepared from HEK293T cells co-transfected with expression vectors for V5-WT NEK3 and constitutively active MEK1 (CA-MEK1; S218D/S222D), as indicated. Immunoprecipitated V5-WT NEK3 was incubated with λ-PPase *in vitro* prior to Western blotting analysis with p-NEK3 (T165) antibodies; α-V5 antibodies detected total NEK3 expression levels. WCL were immunoblotted with antibodies directed against α-MEK1 (to detect CA-MEK1) and α-p-ERK1/2 (T202/Y204) (to show MEK1 downstream activation); α-tubulin was used as a protein loading control. The *graph* shows the relative densitometric quantification of Western blot band intensities for the ratio of p-NEK3 (T165) normalized to total NEK3 levels detected with the α-V5 antibody. *, $p \leq 0.05$; ANOVA was followed by Tukey's multiple comparison test. Western blots are representative of three independent experiments. *H* and *I,* NEK3 catalytic activity is dispensable for phosphorylation at Thr-165 in response to CA-MEK1. Cell lysates were prepared from HEK293T cells co-transfected with expression vectors for either V5-NEK3 wild-type (*WT*) or kinase-inactive NEK3 (D145A) and constitutively active MEK1 (CA-MEK1; S218D/S222D), as indicated. V5-NEK3 constructs were immunoprecipitated (*IP*) with α-V5 antibodies, and NEK3 phosphorylation was examined by Western blotting with α-p-NEK3 (T165) antibodies; α-V5 antibodies detected similar expression levels of the NEK3 constructs. WCLs were immunoblotted with antibodies directed against α-MEK1 (to detect CA-MEK1) and α-pERK1/2 (T202/Y204) (to show MEK1 downstream activation). α-Tubulin was used as a loading control. The *graph* shows the relative densitometric quantification of Western blot band intensities for the ratio of p-NEK3 (T165) normalized to total NEK3 levels detected with the α-V5 antibody. *, $p \leq 0.05$, *n.s.* $p > 0.05$; ANOVA was followed by Tukey's multiple comparison test. Western blots are representative of four independent experiments.

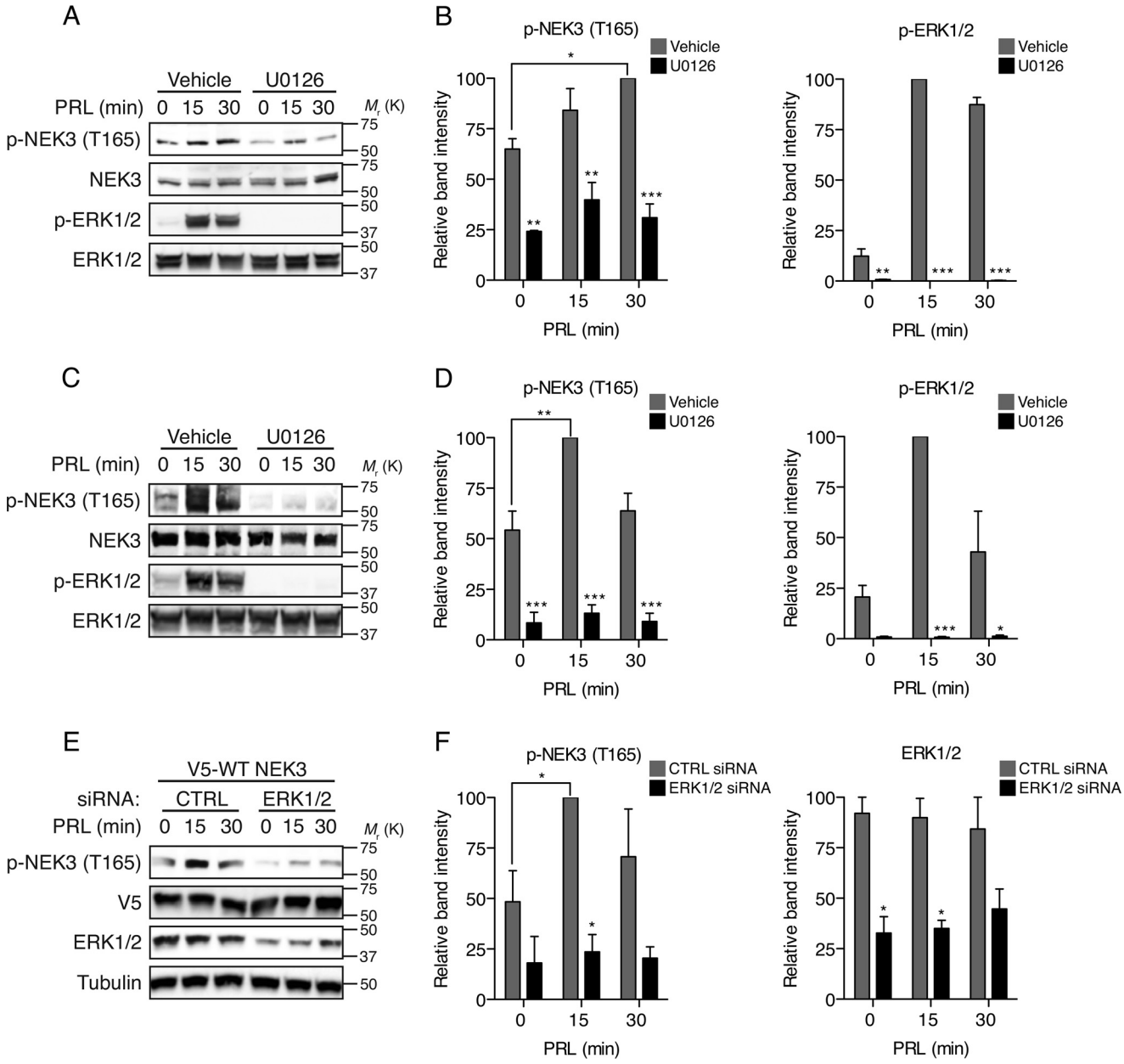

FIGURE 4. **Activation of the PRL-MEK1/2-ERK1/2 signaling pathway in breast cancer cells increases NEK3 Thr-165 phosphorylation.** *A–D,* PRL-induced phosphorylation of endogenous NEK3 at Thr-165 is sensitive to U0126 treatment. Serum-starved T-47D (*A* and *B*) and MCF-7 (*C* and *D*) cells were pre-treated with either dimethyl sulfoxide (*DMSO*) control (*Vehicle*) or U0126 (40 μM) for 2 h and were subsequently stimulated with PRL (250 ng/ml) for the indicated times. Western blotting analysis of endogenous NEK3 phosphorylated at Thr-165 was performed using α-p-NEK3 (T165) antibodies. Lysates were subsequently blotted with α-p-ERK1/2 (T202/Y204) antibodies to confirm inhibition of compound target. Expression of total ERK1/2 served as a protein loading control. *Graphs* show relative densitometric quantification of Western blot band intensities for the ratio of p-NEK3 (T165) normalized to total NEK3 levels (*left panels*) and the ratio of p-ERK1/2 (T202/Y204) normalized to total ERK levels (*right panels*). *, $p \leq 0.05$; **, $p \leq 0.01$; ***, $p \leq 0.001$; ANOVA was followed by Bonferroni's multiple comparison test. Western blot images are representative of three independent experiments. *E* and *F,* PRL-induced NEK3 phosphorylation at Thr-165 is attenuated after knockdown of *ERK1/2* in T-47D cells. T-47D cells stably expressing V5-WT NEK3 were transfected with 50 nM control siRNA (*CTRL*) or ERK1/2 siRNA and incubated for 24 h prior to serum-starvation for 24 h. Cells were stimulated with PRL (250 ng/ml) for the times as indicated. Lysates were immunoblotted with α-p-NEK3 (T165) antibodies; α-tERK1/2 antibodies were used to confirm knockdown. Tubulin was used as a protein loading control. *Graphs* show relative densitometric quantification of Western blot band intensities for the ratio of p-NEK3 (T165) normalized to total NEK3 levels (*F*, *left panel*) and the level of total ERK1/2 expression normalized to tubulin (*F*, *right panel*). *, $p \leq 0.05$; ANOVA was followed by Bonferroni's multiple comparison test. Western blot images are representative of two independent experiments.

and *J*). Expression of *NEK3* cDNA engineered to contain synonymous mutations in the shNEK3-targeting sequence (WT Rescue) was able to partially rescue the cell motility defect caused by knockdown of NEK3 (Fig. 5, *I* and *J*). However, expression of a rescue construct that contained an additional phospho-deficient mutation at Thr-165 (T165V Rescue) remained inhibited to a similar level as the shNEK3 cells (Fig. 5, *I* and *J*). The protein expression level of the WT and T165V rescue constructs was verified to be relatively equivalent by Western blotting analysis (Fig. 5*K*). These data suggest that NEK3 plays a role in the regulation of the focal adhesion complex and is required for efficient cell migration.

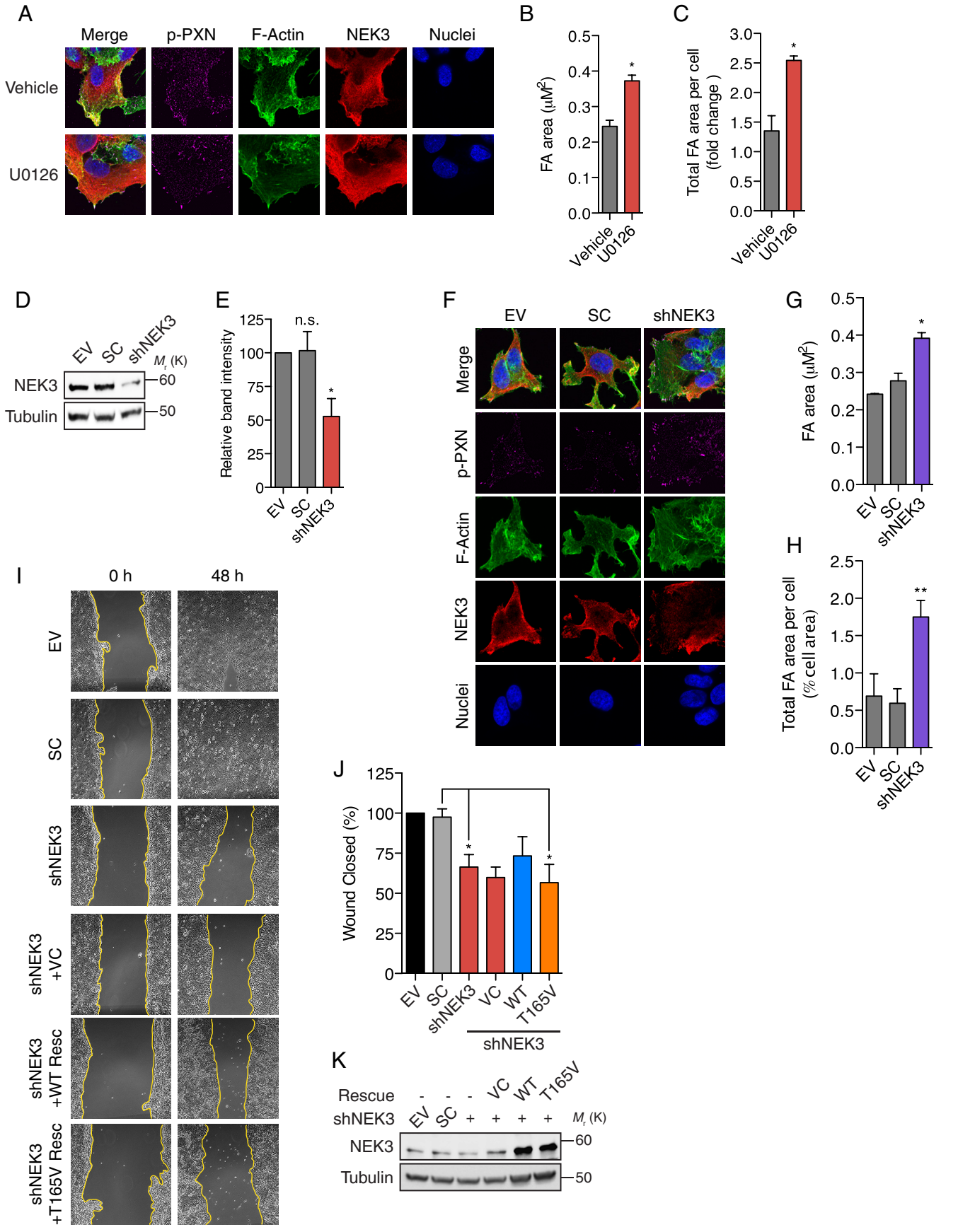
A
Merge
p-PXN
F-Actin
NEK3
Nuclei
Vehicle
U0126
B
FA area (μM²)
Vehicle
U0126
C
Total FA area per cell (fold change)
Vehicle
U0126
D
EV
SC
shNEK3
Mr (K)
NEK3
Tubulin
60
50
E
Relative band intensity
n.s.
EV
SC
shNEK3
F
EV
SC
shNEK3
Merge
p-PXN
F-Actin
NEK3
Nuclei
G
FA area (μM²)
EV
SC
shNEK3
H
Total FA area per cell (% cell area)
EV
SC
shNEK3
I
0 h
48 h
EV
SC
shNEK3
shNEK3 +VC
shNEK3 +WT Resc
shNEK3 +T165V Resc
J
Wound Closed (%)
EV
SC
shNEK3
VC
WT
T165V
shNEK3
K
Rescue
shNEK3
EV
SC
VC
WT
T165V
Mr (K)
NEK3
Tubulin
60
50

To further dissect the role of NEK3 Thr-165 phosphorylation in the regulation of focal adhesion morphology and cell migration, MCF-7 cells were infected with lentiviruses expressing wild-type and phospho-mutant forms of V5-NEK3 (WT, D145A, T161V, and T165V) or GFP as a control. Relatively equivalent expression levels of WT and mutant NEK3 proteins were detected in the stable MCF-7 cells by RT-PCR analysis as well as by Western blotting of cell lysates with an anti-NEK3 antibody (Fig. 6*A*). To evaluate the role of NEK3 phosphorylation at Thr-165 on breast cancer cell migration, stable MCF-7 cells stably expressing V5-WT NEK3 or the phospho-mutant forms of NEK3 were assayed for motility by scratch wound-closure assay. Compared with the MCF-7-GFP control cells, overexpression of the WT NEK3 or the NEK3-T161V mutant did not result in any significant changes to cell motility (Fig. 6*B*). In contrast, the NEK3-T165V mutant significantly inhibited cell motility by 40% compared with cells expressing WT NEK3, and they functioned equivalent to kinase-inactive NEK3-D145A (Fig. 6, *B* and *C*). Importantly, NEK3-T165V was also found to inhibit wound closure when these experiments were performed in the presence of mitomycin-C, an inhibitor of DNA synthesis (data not shown), suggesting that the impairment in the ability to close the wound was likely not attributable to differences in cell proliferation. Thus, NEK3 regulates breast cancer cell migration and is dependent on phosphorylation at Thr-165.

Next, actin filaments and focal adhesions were visualized by indirect immunofluorescent confocal microscopy in the stable MCF-7 cells expressing WT NEK3, NEK3-T161V, or NEK3-T165V using phalloidin and PXN phosphorylated at Tyr-118 (p-PXN), respectively. The localization of exogenous NEK3 proteins were visualized by staining PRL-stimulated MCF-7 cells with α-V5 antibodies (*red*) and was found to be predominantly cytoplasmic (Fig. 6*D*), which is consistent with previously published reports in both fibroblasts (29) and neurons (30). No differences in NEK3 localization were observed between wild-type NEK3 and the phospho-mutants (NEK3-T161V or NEK3-T165V), which all showed enriched staining at the cell periphery and strong co-localization with actin in membrane ruffles (Fig. 6*D*). Expression of NEK-T165V in MCF-7 cells resulted in a dramatic change to the actin cytoskeleton and induced a robust increase in actin stress fibers (Fig. 6*D*). Actin stress fibers are often associated with mature focal adhesion structures. Therefore, to determine whether phosphorylation of NEK3 at Thr-165 plays a role in focal adhesion maturation, we analyzed focal adhesion size by confocal microscopy in MCF-7 cells expressing the various NEK3 constructs. Expression of NEK3-T165V promoted the formation of larger, more intensely stained focal adhesions compared with cells expressing wild-type NEK3 (Fig. 6, *E* and *F*). Importantly, Western blotting analysis determined that the total protein levels of PXN phosphorylated at Tyr-118 and total PXN remained relatively equivalent among the stable NEK3 MCF-7 cells (data not shown).

Focal adhesion structures were also assessed by confocal microscopy, using another protein marker, zyxin. Zyxin, an α-actinin and stress fiber binding protein, is present in mature focal adhesions but is typically absent from small focal complexes (54). Few zyxin-positive adhesions were detected in parental control, wild-type NEK3, or NEK3-T161V cells, indicating the likely presence of focal complexes (Fig. 6, *G* and *I*). In marked contrast, zyxin-positive adhesions were increased by 70% in cells expressing NEK3-T165V compared with WT NEK3 cells under PRL-stimulated conditions (Fig. 6*I*). Size, another marker of focal adhesion maturity, was ~40% greater in NEK3-T165V cells compared with wild-type NEK3 cells (Fig. 6*H*). Importantly, Western blotting analysis determined that the total protein levels of zyxin remain unchanged (data not

FIGURE 5. **NEK3 depletion in breast cancer cells leads to altered focal adhesion morphology and inhibits cell motility.** *A,* pharmacological inhibition of MEK1/2-ERK1/2-mediated signaling induces changes to focal adhesion morphology. Stable MCF-7 cells expressing V5-WT NEK3 were pre-treated with DMSO vehicle control (*Vehicle*) or U0126 (10 μM) for 48 h and were subsequently stimulated with PRL (500 ng/ml) for 15 min. Cells were processed for indirect immunofluorescence using α-V5 antibodies to detect exogenous NEK3 (*red*), FITC-phalloidin to visualize F-actin (*green*), α-phospho-PXN (Tyr-118) antibodies to visualize focal adhesions (*magenta*), and DAPI to visualize the nucleus (*blue*). Cells were imaged using confocal microscopy. *Scale bar,* 10 μM. *B* and *C,* quantification of FA parameters obtained in *A* using antibodies directed against p-PXN to mark the focal adhesion complex. Individual FA area (*B*) and total FA area per cell normalized to cell area (*C*) are presented as the mean ± S.E. of two independent experiments (where each experiment analyzed 10–23 cells and 80–937 focal adhesions per condition). *C*, data are presented as the fold change relative to vehicle control cells. *, $p \leq 0.05$ compared with vehicle control; Student's *t* test. *D* and *E,* knockdown of endogenous NEK3 in MCF-7 cells. Immunoblot analysis (*D*) and quantification (*E*) of NEK3 protein levels in MCF-7 cells stably infected with shRNA vectors targeted to NEK3 (*shNEK3*), scrambled non-targeting negative control (*SC*), or EV negative control. Whole cell lysates were probed with NEK3 antibodies and tubulin served as a protein loading control. The *graph* shows the ratio of the signal intensities of NEK3 normalized to tubulin. *E*, values are presented relative to the empty vector control, which is set as 100%. Data are the mean ± S.E. of four independent experiments. *, $p \leq 0.05$ compared with empty vector and scrambled controls; ANOVA was followed by Tukey's multiple comparison test. Western blots are representative of four independent experiments. *F,* stable MCF-7 cells expressing EV control, scrambled non-targeting control (*SC*), or shRNA targeted to NEK3 (shNEK3) were treated with PRL (500 ng/ml) for 15 min, fixed, and stained for indirect immunofluorescence using α-NEK3 antibodies to detect endogenous NEK3 (*red*), FITC-phalloidin to visualize F-actin (*green*), α-phospho-PXN (Tyr-118) antibodies to visualize focal adhesions (*magenta*), and DAPI to visualize the nucleus (*blue*). Cells were imaged using confocal microscopy. *Scale bar,* 10 μM. *G* and *H,* quantification of FA parameters obtained in *F* using phospho-PXN to mark the FA complex. Individual FA area (*G*) and total FA area per cell normalized to cell area (*H*) are presented as the mean ± S.E. of two independent experiments (where each experiment analyzed 5–21 cells and 115–650 focal adhesions per condition). *, $p \leq 0.05$; **, $p \leq 0.01$ compared with empty vector and scrambled controls. ANOVA was followed by Tukey's multiple comparison test. *I*, cell migration was evaluated by wound healing assay of NEK3 depleted cells. Confluent monolayers of stable MCF-7 cells expressing empty vector control (*EV*), scrambled non-targeting control (*SC*), or shRNA targeted to NEK3 (*shNEK3*) were scratched with a sterile pipette tip and allowed to migrate for 48 h. *NEK3* expression was rescued by transfection of the stable shNEK3 cells with *NEK3* cDNA engineered to contain five synonymous mutations in the shNEK3 target sequence (*WT-Rescue* or *T165V-Rescue*) with empty vector control (*VC*). Representative phase-contrast images captured at 0 and 48 h after wounding are shown. The *solid yellow line* indicates the wound edge. *J,* distance the cells migrated after 48 h relative to the initial wound (0 h) was measured with ImageJ software (National Institutes of Health). Data are presented as the mean ± S.E. of three independent experiments (where each group had at least three technical replicates per experiment). Data are presented relative to the empty vector control, which is set as 100%. *, $p \leq 0.05$ compared with scrambled control (shown in figure); SC *versus* WT Rescue, *n.s.*, $p > 0.05$; ANOVA was followed by Bonferroni's multiple comparison test. *K*, confirmation of NEK3 rescue constructs expression in MCF-7 shNEK3 cells. MCF-7 cells that were stably transduced with shNEK3 were transfected with NEK3 rescue constructs where *NEK3* cDNA was engineered to contain five synonymous mutations in the shNEK3 target sequence (*WT-Rescue*), a NEK3 rescue construct additionally containing the T165V mutation (*T165V Rescue*), or the vector control (*VC*). The expression of the NEK3 rescue constructs (WT Rescue and T165V Rescue) was detected by immunoblot analysis using a NEK3 antibody to show the resistance of the constructs to NEK3 shRNA. Tubulin served as a protein loading control. Western blots are representative of two independent experiments.

shown) among the stable NEK3 MCF-7 cells. Collectively, these data raise the exciting possibility that PRL-MEK1-ERK1/2 targeted phosphorylation at NEK3 Thr-165 plays a critical role in focal adhesion maturation and/or focal adhesion turnover, thereby regulating breast cancer cell migration.

Discussion

In this report, we investigated how activation segment phosphorylation contributes to the activation and function of NEK3 *in vitro*, as well as in breast cancer cells *in vivo*. Phosphorylation within the kinase activation segment, either by autophosphorylation or phosphorylation by an upstream kinase, is an important regulatory mechanism for kinase activation; however, there is presently little known about how phosphorylation regulates the activation of NEK3. Site-directed mutagenesis of Ser/Thr residues (Ser-148, Ser-153, Thr-161, and Thr-165) within the NEK3 activation segment identified NEK3 Thr-165 as a major site of autophosphorylation *in vitro* (Figs. 1, *F* and *G*, and

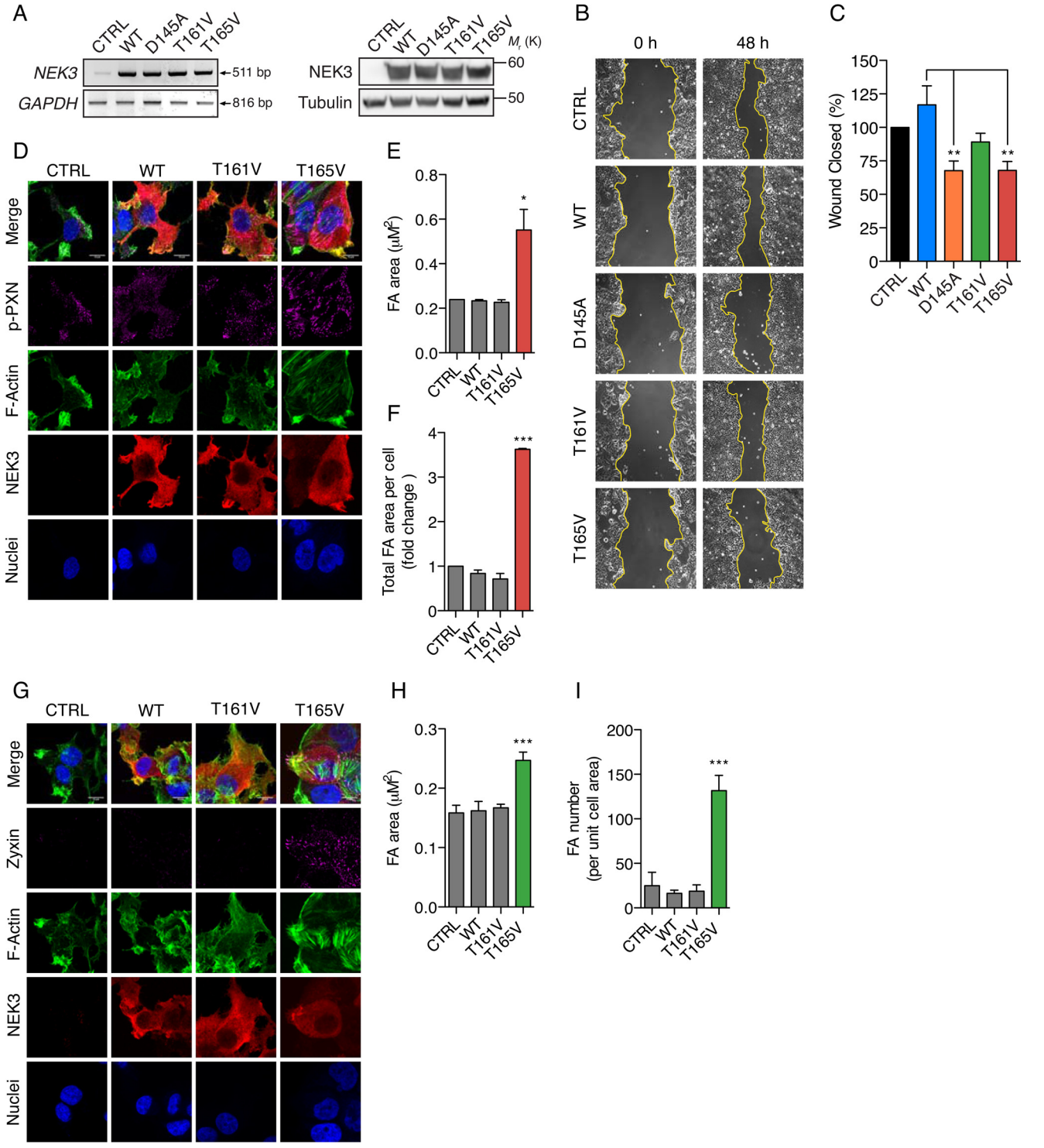

2, *E* and *F*), as well as being required for its catalytic activity *in vitro* (Fig. 1, *H* and *I*). To our knowledge, this is the first *in vitro* autophosphorylation site described for NEK3. The proximity of the Thr-161 and the Thr-165 sites raises the possibility that phosphorylation at these residues could be coordinately regulated. Indeed, we found that replacement of Thr-161 with a non-phosphorylatable valine residue (T161V) resulted in a moderate reduction of phosphorylation at Thr-165 (Fig. 2, *G* and *H*). This leads to several possible scenarios, including that phosphorylation at NEK3 Thr-161 may serve as a priming event that is required for maximal phosphorylation at Thr-165. However, it does not exclude the possibility that replacement of the Thr-161 site with a valine residue could alter the structure of the NEK3 activation loop, rendering it more accessible for autophosphorylation at Thr-165. Generation of a phosphospecific antibody specific for phosphorylation at the Thr-161 site would allow for future studies dissecting the potential interplay between these two sites in the phosphoregulation of NEK3 activation. Interestingly, the residues surrounding residue Thr-161 of NEK3 fit the very loose phosphorylation consensus sequence of the NEK founding member, NIMA (F/L)*XX*(S/T) (^{158}FAC**T**^{161}) (55), lending support to the notion that phosphorylation at this site could have the potential to be an autocatalytic event. Furthermore, crystal structure analysis where NEK3 is phosphorylated on residues Thr-161 and/or Thr-165 will clarify the mechanism of how phosphorylation at these site(s) regulates NEK3 activation.

Both the Thr-161 and the Thr-165 sites are highly conserved among NEK family members (Fig. 1*E*), and several studies have examined how phosphorylation at corresponding sites within the activation segment contributes to the activation of other NEK family members. NEK3 Thr-161 aligns with the corresponding Thr-175 on NEK2 kinase, Ser-206 on NEK6 kinase and Ser-195 on NEK7 kinase. Previous work has demonstrated that phosphorylation of each of these residues is important in regulating the activation of each of the respective NEK kinases (26, 35). This is in contrast to our results, which instead demonstrated a key regulatory role for phosphorylation at the NEK3 Thr-165 site, revealing a unique difference in the regulation of NEK3 activation compared with its family members. NEK3 Ser-148 and Ser-153 are much less conserved among NEK family members (Fig. 1*E*), and individual mutation of these serine residues resulted in either a modest reduction or equivalent level of autophosphorylation compared with wild-type NEK3, respectively (Fig. 1, *F* and *G*). This suggests that these serine residues are unlikely to function as regulatory autophosphorylation sites *in vitro* and were therefore not included for further analysis in this study. However, it is reasonable to postulate that additional regulatory phosphorylation sites, both within the N-terminal kinase domain as well as in the C-terminal non-enzymatic region of the protein, remain to be identified.

Our previous data demonstrated that PRL stimulates the catalytic activity of NEK3 (24); however, the mechanism was not identified. In this report, it was demonstrated that endogenous NEK3 is phosphorylated at Thr-165 in response to PRL stimulation in breast cancer cells (Fig. 4, *A–D*). The kinetics of NEK3 phosphorylation in breast cancer cell lines stimulated with PRL occurs within 15–30 min (Fig. 4, *A–F*). However, NEK3 autophosphorylation *in vitro* is slower, with maximum autophosphorylation occurring between 45– 60 min (Fig. 1, *A* and *B*). These observations suggested that additional mechanisms might exist *in vivo* that could contribute to more rapid phosphorylation and activation of NEK3. In addition, it was observed that the catalytic activity of NEK3 was dispensable for phosphorylation at NEK3 Thr-165 in cells, as the kinase-inactive D145A mutant was phosphorylated to a similar level as WT NEK3 in response to PRL stimulation (Fig. 3, *A* and *B*). Therefore, the possibility that phosphorylation at NEK3 Thr-165 could be targeted by an independent upstream kinase was examined. Our data revealed that NEK3 Thr-165 represents a potential novel ERK1/2-mediated phosphorylation site. This was supported by data showing that inhibition of ERK1/2 activation in breast cancer cells, both by pharmacological inhibition and ERK1/2-specific siRNA, resulted in significant attenuation of phosphorylation at NEK3 Thr-165 (Fig. 4). This is the first report of any specific kinase contributing to the phosphorylation of NEK3. Moreover, a novel interaction between NEK3 and ERK1/2 was demonstrated using co-immunoprecipitation approaches (Fig. 3*D*). This suggested the possibility that ERK1/2 may directly phosphorylate NEK3 at Thr-165, addi-

FIGURE 6. **Phosphorylation at NEK3 Thr-165 modulates focal adhesion morphology to regulate breast cancer cell migration.** *A*, analysis of *NEK3* mRNA and protein levels in MCF-7 cells expressing *NEK3* cDNA. MCF-7 cells were transduced with *NEK3* cDNA (wild-type and phospho-mutants) by lentiviral infection. Total RNA and whole cell lysates were isolated from cells and subjected to RT-PCR (*left panel*) or immunoblot analysis (*right panel*). GAPDH and tubulin served as loading controls, respectively. *bp*, indicates base pairs. Data are representative of two independent experiments. *B,* cell migration evaluated by wound healing assay. Confluent monolayers of stable MCF-7 cells expressing the indicated V5-NEK3 phospho-mutant constructs were scratched with a sterile pipette tip and allowed to migrate for 48 h. Representative phase-contrast images captured at 0 and 48 h after wounding are shown. The *solid yellow line* indicates the wound edge. *C*, distance the cells migrated after 48 h relative to the initial wound (0 h) was measured with ImageJ software (National Institutes of Health). Data are presented as the mean ± S.E. of three independent experiments (where each group had at least three technical replicates per experiment). Data are presented relative to the parental GFP control group, which is set as 100%. **, $p \leq 0.01$ compared with WT NEK3 (indicated in figure); *CTRL versus* WT, $p > 0.05$; WT *versus* T161V, $p > 0.05$; ANOVA was followed by Bonferroni's multiple comparison test. *D*, MCF-7 cells expressing V5-NEK3 (wild-type and phospho-mutants) or parental control cells (*CTRL*) were stimulated with PRL (500 ng/ml) for 15 min, fixed, and stained for indirect immunofluorescence using α-V5 antibodies to detect exogenous NEK3 (*red*), FITC-phalloidin to visualize F-actin (*green*), α-phospho-PXN (Tyr-118) antibodies to visualize focal adhesions (*magenta*), and DAPI to visualize the nucleus (*blue*). Cells were imaged using confocal microscopy. *Scale bar,* 10 μM. *E* and *F,* quantification of FA parameters obtained in *D* using phospho-PXN to mark the FA complex. Individual FA area (*E*) and total FA area per cell normalized to cell area (*F*) are presented as the mean ± S.E. of two independent experiments (where each experiment analyzed 3–22 cells and 231–1377 focal adhesions per condition). *F*, data are presented relative to the parental control, which is arbitrarily set to 1. *, $p \leq 0.05$; ***, $p \leq 0.001$ compared with WT NEK3; ANOVA was followed by Bonferroni's multiple comparison test. *G*, MCF-7 cells expressing V5-NEK3 (wild-type and phospho-mutants) or parental control cells (*CTRL*) were treated with 500 ng/ml PRL for 15 min, fixed, and stained for indirect immunofluorescence using α-V5 antibodies to detect exogenous NEK3 (*red*), FITC-phalloidin to visualize F-actin (*green*), α-zyxin antibodies to visualize focal adhesions (*magenta*), and DAPI to visualize the nucleus (*blue*). Cells were imaged using confocal microscopy. *Scale bar,* 10 μM. *H* and *I,* quantification of FA parameters obtained in *G* using α-zyxin antibodies to mark the FA complex. Individual FA area (*H*) and FA number normalized to cell area (*I*) are presented as the mean ± S.E. of two independent experiments (where each experiment analyzed 3–24 cells and 4 –1181 focal adhesions per condition). ***, $p \leq 0.001$ compared with WT NEK3; ANOVA was followed by Bonferroni's multiple comparison test.

tionally supported by analysis indicating that Thr-165 falls within an ERK1/2 consensus phosphorylation sequence. Preliminary studies by our laboratory indicate that ERK1/2 may require additional scaffolding proteins and/or co-factor(s) to facilitate phosphorylation of NEK3 at Thr-165 *in vitro* (data not shown).

The functional consequences of phosphorylation at Thr-165 were examined by expression of the phospho-deficient NEK3 mutant (NEK3-T165V) in MCF-7 breast cancer cells. Our findings demonstrated that expression of NEK3-T165V resulted in increased focal adhesion area (Fig. 6, *D–F*), increased presence of zyxin-positive focal adhesions (Fig. 6, *G–I*), reorganization of the actin cytoskeleton into stress fibers (Fig. 6*D*), with a concordant impairment in cell motility (Fig. 6, *B* and *C*). Functionally, the dominant-negative effect of the phospho-deficient NEK3-T165V mutant was recapitulated through knockdown of endogenous NEK3 expression by shRNA (Fig. 5, *F–J*) and through inhibition of the MEK/ERK1/2 signaling pathway (Fig. 5, *A–C*). Importantly, ERK1/2 have an established role regulating cell migration in many cell types (56–59), including breast cancer cells (60, 61). Collectively, these data suggest that phosphorylation at NEK3 Thr-165, likely in response to activation of ERK1/2 signaling, regulates focal adhesion maturation and/or disassembly thereby influencing cell migration. There are several possibilities as to how NEK3 could regulate disassembly of the focal adhesion complex. Focal adhesions connect the actin cytoskeleton of the cell to the extracellular matrix through integrins, which are known to be key regulators of cell migration and invasion. Integrins localize to FAs and recruit focal adhesion proteins such as paxillin, vinculin, and focal adhesion kinase to trigger the downstream activation of the RHO family of GTPases (24, 62, 63). Our laboratory previously demonstrated that there is a PRL-dependent association between the PRLR and β1 integrin (64), as well as between PRLR and NEK3 (24), with both interactions reaching maximal levels upon 15 min of PRL stimulation. This suggests the possibility that NEK3 could also be in complex with β1 integrin and could regulate its activation either through direct phosphorylation of its cytoplasmic tail or through phosphorylation of β1 integrin-binding partner(s) of the focal adhesion complex. The phosphorylation of integrin cytoplasmic tails has been proposed to be an important mechanism to regulate the activation and function of integrins (65), and there is precedence for Ser/Thr kinase-mediated phosphorylation of the cytoplasmic tail of β-integrins resulting in promoting cell migration (66). Furthermore, NEK3 has been shown to regulate the serine phosphorylation of PXN (12), which has been previously reported to regulate adhesion turnover in migrating cells (67). Therefore, NEK3-mediated phosphorylation of PXN and its role in the regulation of FA turnover merits further study. However, this does not limit the possibility that NEK3 may additionally interact with and regulate phosphorylation of other components of the focal adhesion complex.

The coordinated assembly and disassembly of the focal adhesion complex is crucial to directed cell migration (53, 68). Focal adhesion dynamics and cell migration are largely controlled by RHO GTPases (RAC, RHO, and CDC42). RAC and RHO must be reciprocally activated, either spatially or temporally, in order for efficient cell migration to occur (22, 69–71). Collectively, the phenotype observed in cells expressing NEK3-T165V is reminiscent of activation of the RHO pathway. How might phosphorylation at NEK3 Thr-165 regulate the RHO pathway? Our work previously identified a regulatory role for wild-type NEK3 promoting the activation of RAC1, with data suggesting that NEK3 modulates phosphorylation of the guanine nucleotide exchange factor (GEF), VAV2, leading to activation of RAC1. RAC and RHO are positively regulated by GEFs that promote GTP binding and are down-regulated by GTPase-activating proteins (GAPs) that stimulate the intrinsic GTPase activity of RAC/RHO. To date, there are ~70 GEFs and 80 GAPs that have been identified for RHO GTPases, which can have antagonistic effects on the activities of RAC and RHO. Therefore, it is possible that NEK3 could regulate GEFs and/or GAPs to alter the balance between RAC and RHO signaling. VAV2 is known to act as a GEF for both RAC and RHO proteins, so it is also plausible that NEK3-mediated phosphorylation of VAV2 could alter its specific localization within the cell or its interaction with RAC or RHO depending on signaling cues to promote cell migration. Identification of biologically relevant direct substrates of NEK3 will greatly aid in the dissection of the role of NEK3 in regulating these processes. Collectively, these data provide novel mechanistic insight into the role of NEK3 activation and function in breast cancer cells, and as a targetable kinase it has potential therapeutic implications in the treatment of breast cancer.

Experimental Procedures

Reagents—U0126 (1,4-diamino-2,3-dicyano-1,4-bis(2-aminophenylthio)butadiene; catalog no. 9903), nonradioactive ATP (catalog no. 9804), and mouse mAb IgG XP isotype controls (catalog no. 5415) were obtained from Cell Signaling Technology (Danvers, MA). λ-PPase (catalog no. 14-405), protease inhibitor mixture set III, EDTA-free (catalog no. 539134), and phosphatase inhibitor mixture set I (catalog no. 524624) were purchased from EMD Millipore (Billerica, MA). Phosphorylated NEK3 peptides (pT161 and pT165) were purchased from New England Peptide (Gardner, MA). Recombinant protein G-agarose beads (catalog no. 15920-010) and Coomassie SimplyBlue SafeStain (catalog no. LC6060) were from Life Technologies, Inc. (Carlsbad, CA). Prolactin (PRL) was gifted by Dr. Anthony Kossiakof (University of Chicago, Chicago, IL). Nonidet P-40 (catalog no. N3500) and Triton X-100 (catalog no. A16046) were from United States Biological (Salem, MA) and Alfa Aesar (Ward Hill, MA), respectively. Unless otherwise specified, all chemicals were purchased from Sigma.

Cell Culture and Transfection—T-47D and MCF-7 human breast cancer cell lines were obtained from the American Type Culture Collection (ATCC; Manassas, VA) and cultured in Dulbecco's modified Eagle's medium (DMEM; Life Technologies, Inc.) supplemented with 10% FBS (Sigma), 100 units/ml penicillin/streptomycin (Life Technologies, Inc.), and 1 μg/ml ciprofloxacin (Corning Inc.). Human embryonic kidney 293T (HEK293T) cells were provided by Dr. Debabrata Chakravarti (Northwestern University, Chicago, IL), and the Phoenix-AMPHO retroviral packaging cells were provided by Dr. Jonathan Licht (Northwestern University, Chicago, IL) and were cultured in DMEM with 10% FBS. All cells were cultured on tissue

TABLE 1
List of primers for site-directed mutagenesis

Primer name		Sequence (5′–3′)
MEK1 S218D/S222D	Forward	AGCTCATCGACGACATGGCCAACGACTTCGTGGGCACAAG
	Reverse	CTTGTGCCCACGAAGTCGTTGGCCATGTCGTCGATGAGCTGCCC
NEK3 D145A	Forward	AAAAGTGAAATTGGGAGCCTTTGGATCTGCCCGTC
	Reverse	GACGGGCAGATCCAAAGGCTCCCAATTTCACTTTT
NEK3 K33R	Forward	CAGTAATCAGATGTTTGCCATGCGAGAAATAAGGCTTCCCAAGTCT
	Reverse	AGACTTGGGAAGCCTTATTTCTCGCATGGCAAACATCTGATTACTG
NEK3 D127A	Forward	GAAACGTGTGCTACACAGAGCTATCAAGTCCAAGAATATCT
	Reverse	AGATATTCTTGGACTTGATAGCTCTGTGTAGCACACGTTTC
NEK3 S148A	Forward	ATTGGGAGACTTTGGAGCTGCCCGTCTTCTCTC
	Reverse	GAGAGAAGACGGGCAGCTCCAAAGTCTCCCAAT
NEK3 S153A	Forward	CTGCCCGTCTTCTCGCCAATCCGATGGCA
	Reverse	TGCCATCGGATTGGCGAGAAGACGGGCAG
NEK3 T161V	Forward	CAATCCGATGGCATTTGCTTGTGTCTATGTGGGAACTCCTTATTAT
	Reverse	ATAATAAGGAGTTCCCACATAGACACAAGCAAATGCCATCGGATTG
NEK3 T165V	Forward	TGGCATTTGCTTGTACCTATGTGGGAGTTCCTTATTATGTGCC
	Reverse	GGCACATAATAAGGAACTCCCACATAGGTACAAGCAAATGCCA
NEK3 T165A	Forward	GCTTGTACCTATGTGGGAGCTCCTTATTATGTGCCTC
	Reverse	GAGGCACATAATAAGGAGCTCCCACATAGGTACAAGC
NEK3 T165S	Forward	GCTTGTACCTATGTGGGATCTCCTTATTATGTGCCTC
	Reverse	GAGGCACATAATAAGGAGATCCCACATAGGTACAAGC
NEK3 T165E	Forward	GGCATTTGCTTGTACCTATGTGGGAGAGCCTTATTATGTGCCTCC
	Reverse	GGAGGCACATAATAAGGCTCTCCCACATAGGTACAAGCAAATGCC
NEK3 shRNA rescue	Forward	GACTTTGGATCTGCCCGTCTTCTCAGTAACCCTATGGCATTTGCTTGTACCTATGTG
	Reverse	CACATAGGTACAAGCAAATGCCATAGGGTTACTGAGAAGACGGGCAGATCCAAAGTC

culture-treated polystyrene from Falcon (Corning Inc.) in a humidified 37 °C incubator containing 5% CO_2. For PRL treatment, cells were deprived of serum for 18–24 h in phenol red-free medium, followed by addition of PRL to yield a final concentration of 250 or 500 ng/ml (indicated in figure legend). For transfection, a ratio of 2 μg of plasmid DNA was mixed with 5 μl of Lipofectamine LTX reagent (Life Technologies, Inc.) following the manufacturer's recommendations. Cells were typically analyzed 48 h post-transfection. Cell lines were regularly tested to be free from mycoplasma contamination using MycoAlert *Mycoplasma* detection kit (Lonza Inc., Walkersville, MD).

RNA Interference—SignalSilence p44/42 MAPK (ERK1/2) siRNA (catalog no. 6560) and SignalSilence Non-Targeting Control siRNA (catalog no. 6568S) were purchased from Cell Signaling Technology. MCF-7 breast cancer cells were transfected with the siRNA at a final concentration of 50 nM using RNAiMax (Life Technologies, Inc.) following the manufacturer's protocol. Transfected cells were analyzed 60–72 h post-transfection. For NEK3 knockdown, pRFP-C-RS HuSH 29-mer constructs containing NEK3 shRNA (shNEK3) (catalog no. TF320430/FI378940; CTCTCCAATCCGATGGCATTTGCTTGTAC), empty vector (EV) (catalog no. TR30014), and scrambled (SC) non-targeting control (catalog no. TR30015; GCACTACCAGAGCTAACTCAGATAGTACT) were purchased from Origene (Rockville, MD).

Constructs and Viruses—Full-length human *NEK3* cDNA (accession catalog no. BC019916) was PCR-amplified using Platinum *Taq* High Fidelity DNA polymerase (Life Technologies, Inc.) from cDNA purchased from Open Biosystems Inc. (Clone ID, 5000918; Lafayette, CO) using the following primers (For, 5′-GGGGTACCGAGCCACCATGGATGACTACATGGTC-3′, and Rev, 5′-AATTTGCGGCCGCCATCTGTCGCACAGGCCTTG-3′). *NEK3* cDNA was cloned into the pcDNA3.1/*myc*-His A vector (Life Technologies, Inc.) containing C-terminal *myc* and His_6 epitope tags using KpnI and NotI restriction enzyme sites. NEK3 mutants (D145A, K33R/D127A, T161V, T165V, T165A, T165S, T165E, S148A, and S153A) were constructed using the QuickChange Lightning site-directed mutagenesis kit (Agilent Technologies Inc., Santa Clara, CA) following the manufacturer's protocol. To generate shRNA-resistant cDNA, five silent point mutations were introduced into the shRNA-targeting sequence of the wild-type *NEK3* cDNA using site-directed mutagenesis. pENTR1A-MEK1 (W1) was a gift from Dr. Paul Khavari (Addgene catalog no. 21208; Cambridge, MA), and site-directed mutagenesis was performed to substitute residues Ser-218 and Ser-222 with aspartic acid residues (S218D/S222D) to obtain a constitutively active form of MEK1 (CA-MEK1) (72, 73). pENTR1A-MEK1 S218D/S222D was recombined into the pLenti CMV/TO GFP-Zeo DEST lentiviral destination vector using Gateway LR Clonase II enzyme mix (Life Technologies, Inc.) according to the manufacturer's protocol. pLenti CMV/TO GFP-Zeo DEST was a gift from Dr. Eric Campeau (Addgene; plasmid catalog no. 719-1 (74)). Primer sequences used for site-directed mutagenesis are listed in Table 1. All mutations were confirmed by traditional DNA sequencing at the Genomics Core Facility (Northwestern University, Chicago, IL).

Similarly, PCR-amplified full-length *NEK3* cDNA was cloned into the pENTR4-V5 (w71-3) vector containing an N-terminal V5 epitope tag using KpnI and NotI restriction enzyme sites to generate entry clones. pENTR4-V5 (w71-3) was a gift from Dr. Eric Campeau (Addgene; plasmid catalog no. 17425 (74)). NEK3 mutants were constructed using the QuickChange Lightning site-directed mutagenesis kit (D145A, T161V, and T165V) following the manufacturer's protocol. pENTR4-V5-NEK3 entry clones were recombined into the pLenti CMV/Puro DEST lentiviral destination vector using Gateway LR Clonase II enzyme mix (Life Technologies, Inc.) according to the manufacturer's protocol. pLenti CMV/Puro DEST was a gift from Dr. Eric Campeau (Addgene; plasmid catalog no. 17452 (74)). pLenti CMV/V5-NEK3 plasmids were co-transfected into HEK293T cells with ViraPower lentiviral packaging mix (Life Technologies, Inc.) using Lipofectamine LTX (Life Technologies, Inc.). Supernatants containing NEK3

lentivirus were collected 48 h post-transfection and filtered through a Millex-HV PVDF 0.45 μM filter (EMD Millipore). T-47D and MCF-7 cells were transduced with viral supernatant supplemented with fresh growth medium containing 8 μg/ml Polybrene (EMD Millipore) by spin infection (500 × *g* at 32 °C) for 2 h. Cells stably expressing the pLenti CMV/V5-NEK3 plasmids were selected for by treatment with puromycin (2 μg/ml) for ~2 weeks. Pools of puromycin-resistant cells were used for experiments.

Cell Lysis and Western Blotting—For detection of endogenous NEK3, cells were rinsed in ice-cold PBS and scraped in ice-cold PBS containing 1× protease inhibitor mixture, 2.5 mM EDTA, and 2.5 mM EGTA. Cells were lysed in buffer containing 50 mM HEPES-KOH (pH 7.4), 5 mM $MnCl_2$, 10 mM $MgCl_2$, 5 mM EGTA, 2 mM EDTA, 100 mM NaCl, 5 mM KCl, 0.1% (v/v) Nonidet P-40, 2 mM Na_3VO_4, 20 mM β-glycerophosphate, 20 mM NaF, 1× protease inhibitor mixture, and 1× phosphatase inhibitor mixture. For all other experiments, unless otherwise indicated, cells were rinsed and scraped in ice-cold PBS and subsequently lysed in buffer containing 50 mM Tris (pH 8.0), 5 mM EDTA, 150 mM NaCl, 5% (v/v) glycerol, 1% (v/v) Triton X-100, 50 mM NaF, 2 mM Na_3VO_4, 0.1 M PMSF, 1× protease inhibitor mixture, and 1× phosphatase inhibitor mixture. Lysates were resolved by SDS-PAGE and transferred to PVDF membranes (Bio-Rad). Membranes were blocked with either casein blocker (Thermo Fisher Scientific, catalog no. 37532) or for phospho-specific antibodies, 3% (w/v) BSA (prepared in Tris-buffered saline (TBS) containing 0.1% (v/v) Tween 20) and subsequently incubated with primary antibodies diluted in blocking buffer overnight at 4 °C. Bound antibodies were visualized with HRP-conjugated secondary antibodies against mouse or rabbit IgG using ECL2 Western blotting substrate (Thermo Fisher Scientific). Blots were developed using the FujiFILM LAS-3000 imaging system (Fujifilm Medical Systems, Stamford, CT). Images were initially processed, and densitometric analysis was performed using FujiFILM Multi Gauge Version 3.0 program (Fujifilm Medical Systems). Quantification of blot intensities was performed using data that were obtained within a linear range of exposure.

Antibodies for Western Blotting—The following antibodies were used for Western blotting analysis at the indicated dilutions: mouse monoclonal anti-Myc (catalog no. 2276, 1:1000 dilution), rabbit monoclonal anti-p44/42 MAPK (ERK1/2) (catalog no. 4695, 1:1000 dilution), rabbit monoclonal anti-phospho-p44/42 MAPK (ERK1/2) (Thr-202/Tyr-204) (catalog no. 4370, 1:1000 dilution), rabbit polyclonal anti-MEK1/2 (catalog no. 9122, 1:1000 dilution), rabbit polyclonal anti-phosphothreonine (catalog no. 9381, 1:666 dilution), and rabbit polyclonal anti-phospho-PXN (Tyr-118) (catalog no. 2541, 1:1000 dilution) antibodies were purchased from Cell Signaling Technology. Mouse monoclonal anti-V5 (catalog no. R96025, 1:2500 dilution), mouse monoclonal anti-α-tubulin (catalog no. 32-2500, 1:1000 dilution), rabbit polyclonal anti-phosphoserine (catalog no. 61-8100; 1:125 dilution), and rabbit polyclonal anti-phosphothreonine (catalog no. 71-8200, 1:500 dilution) antibodies were obtained from Life Technologies, Inc. Mouse monoclonal anti-PXN (catalog no. 05-417, 1:1000 dilution) and rabbit polyclonal anti-zyxin (ab71842, 1:1000 dilution) antibodies were from EMD Millipore and Abcam (Cambridge, MA), respectively. Rabbit polyclonal anti-NEK3 (1:1000 dilution) and rabbit polyclonal anti-phospho-NEK3 (Thr-165) (1:666 dilution) antibodies were custom-made by New England Peptide, as described below. HRP-conjugated ECL sheep anti-mouse IgG and donkey anti-rabbit IgG antibodies were from GE Healthcare. HRP-conjugated Clean Blot IP detection reagent was purchased from Thermo Fisher Scientific (Waltham, MA).

Generation of Custom NEK3 Antibodies—A custom polyclonal affinity-purified antibody to phosphorylated NEK3 residue threonine 165, α-p-NEK3 (T165), was generated by New England Peptide. New Zealand White rabbits were immunized against a peptide containing residues 160–170 located within the N-terminal kinase domain of human NEK3 (^{160}CTYVG-(pT)PYYVP^{170}), where (pT) indicates the phosphorylated threonine 165 residue. Subsequently, double affinity purification using the non-phosphorylated and phosphorylated peptide was performed to yield the phosphospecific antibody. Similarly, New England Peptide produced a custom polyclonal antibody that recognizes total NEK3 protein. New Zealand White rabbits were immunized with a peptide to residues 487–496 located within the C terminus of human NEK3 (^{487}NPDWVSELKK^{496}). Affinity purification was performed to yield the purified NEK3 antibody (α-NEK3).

Co-immunoprecipitation Assay—Transfected HEK293T cells were lysed in co-immunoprecipitation buffer (20 mM Tris-HCl (pH 7.5), 150 mM NaCl, 1% (v/v) Nonidet P-40, 100 mM NaF, 5 mM $MgCl_2$, 0.5 mM Na_3VO_4, 1 mM PMSF, 5 mM β-glycerophosphate, 1× protease inhibitor mixture, and 1× phosphatase inhibitor mixture), modified from previously published interaction between RAC1 and ERK1/2 (75). Lysates were precleared with 50 μl of recombinant protein G-agarose beads (50% slurry in PBS) with rotation at 4 °C for 1 h. Pre-cleared lysates were incubated with 3 μg of either IgG isotype control or anti-V5 epitope tag antibodies (Life Technologies, Inc., catalog no. R96025) overnight at 4 °C with rotation. 50 μl of recombinant protein G-agarose beads (50% slurry in PBS) was added to immunocomplexes and rotated at 4 °C for 2 h. Immunoprecipitates were washed three times in lysis buffer, eluted by boiling in 2× Laemmli sample buffer (Bio-Rad) containing 5% (v/v) β-mercaptoethanol, and analyzed by Western blotting.

NEK3 Autophosphorylation Assay—Myc-NEK3 proteins (WT and mutants) were produced by *in vitro* transcription/translation in a rabbit reticulocyte lysate using 2.0 μg of pcDNA3.1/*myc*-His NEK3 plasmid DNA in the TnT Quick-Coupled Transcription/Translation System (Promega, Madison, WI) following the manufacturer's protocol. 450 μl of modified NEB buffer (29) (50 mM HEPES-KOH (pH 7.4), 5 mM $MnCl_2$, 10 mM $MgCl_2$, 5 mM EGTA, 2 mM EDTA, 100 mM NaCl, 5 mM KCl, 0.1% (v/v) Nonidet P-40, 30 μg/ml RNase A, 30 μg/ml DNase I, 1 mM PMSF, 5 mM β-glycerophosphate, 5 mM NaF, 1× protease inhibitor mixture, and 1× phosphatase inhibitor mixture) was added, and Myc-NEK3 was immunoprecipitated using 1 μl of the anti-Myc antibody (Cell Signaling Technology, catalog no. 2276) with rotation overnight at 4 °C. Immune complexes were captured using 50 μl of recombinant protein G-agarose beads (50% slurry in PBS) with rotation at

4 °C for 2 h. Beads were subsequently washed three times in modified NEB buffer and twice in kinase wash buffer (50 mM HEPES-KOH (pH 7.4) and 5 mM $MnCl_2$). Beads were resuspended in 40 μl of kinase buffer (50 mM HEPES-KOH (pH 7.4), 5 mM $MnCl_2$, 5 mM β-glycerophosphate, 5 mM NaF, 1 mM DTT, 200 μM nonradioactive ATP) and incubated at 30 °C for the time point(s) indicated in the figure legends. Kinase reaction was terminated by addition of 2× Laemmli sample buffer containing 5% (v/v) β-mercaptoethanol. Samples were boiled for 5 min and resolved by SDS-PAGE. NEK3 protein phosphorylation was detected by Western blotting analysis using pan anti-phosphothreonine or anti-p-NEK3 (T165) antibodies. To examine NEK3 activation, kinase assays were performed as described above, with the addition of 1.4 mg/ml dephosphorylated casein (Sigma, catalog no. C4032) as substrate added to the reactions.

In Vitro Phosphatase Treatment—Captured NEK3 immunocomplexes were incubated with 400 units of λ-PPase (EMD Millipore) in phosphatase buffer (50 mM HEPES-KOH (pH 7.4), 100 mM NaCl, 2 mM DTT, 0.01% (v/v) Nonidet P-40, 1 mM $MnCl_2$) for 90 min at 30 °C. Phosphatase reactions were terminated by boiling for 5 min in 2× Laemmli sample buffer, and the level of NEK3 phosphorylation was measured by immunoblot analysis using antibodies against p-NEK3 (T165).

RNA Extraction and NEK3 RT-PCR—Total RNA was isolated from MCF-7 cells using the RNeasy Plus mini kit according to manufacturer's instructions (Qiagen; Valencia, CA). cDNA was synthesized with the qScript^{TM} cDNA Supermix kit (Quanta Biosciences, Gaithersburg, MD) using 1 μg of RNA as template for the reaction. NEK3 was amplified using gene-specific primers (For, 5′-CAATAAAAGTGACATCTGGTCCTTGGG-3′, and Rev, 5′-CAGATGGACTGACTTATTACCTTTTTCTTCTC-3′) using GoTaq Hot Start Green Master Mix (Promega). The 511-bp PCR product was visualized on an ethidium bromide-stained 1.5% agarose gel, and an image was captured with FujiFILM LAS-3000 imaging system. The 816-bp product corresponding to glyceraldehyde-3-phosphate dehydrogenase (GAPDH) (For, 5′-TGGCAAATTCCATGGCACCGTCAA-3′ and Rev, 5′-ACCACCCTGTTGCTGTAGCCAAAT-3′) was used as a loading control.

Immunofluorescence Microscopy—MCF-7 cells were cultured on glass coverslips (VWR International, Radnor, PA) for 18 h in full growth medium prior to 24 h of serum starvation. Immunofluorescence staining was performed after PRL treatment (500 ng/ml) for 15 min. Briefly, cells were fixed in 4% (v/v) paraformaldehyde (Electron Microscopy Sciences, Hatfield, PA), permeabilized with 0.05% (v/v) Nonidet P-40 in PBS for 10 min, and blocked with 5% (v/v) goat serum (Life Technologies, Inc., catalog no. 50062Z) in PBS for 1 h. All primary and secondary antibodies were diluted in 2% (v/v) goat serum in PBS. The following primary antibodies were incubated overnight at 4 °C: mouse monoclonal anti-V5 epitope tag (Life Technologies, Inc., catalog no. R96025; 1:100 dilution) or mouse monoclonal anti-NEK3 (Abgent Inc., catalog no. AT3017a; San Diego, CA; 1:75 dilution) were used to detect exogenous or endogenous NEK3, respectively. Rabbit monoclonal anti-phospho-PXN (Tyr-118) (Abcam, catalog no. 32084; 1:100 dilution) or rabbit polyclonal anti-zyxin (Sigma, catalog no. HPA004835; 1:100 dilution) were used to mark the focal adhesion complex. Coverslips were subsequently incubated with Alexa Fluor 568 goat anti-mouse IgG (H+L) and Alexa Fluor 647 goat anti-rabbit IgG (H+L) secondary antibodies (Life Technologies, Inc.; 1:500 dilution) for 1 h at room temperature. Coverslips were counterstained with fluorescein-conjugated phalloidin (1:40; 20 min) to visualize actin filaments, and nuclei were visualized with DAPI (1:1000; 5 min). Coverslips were mounted on slides with ProLong Gold antifade reagent (Life Technologies, Inc.). Images were captured at room temperature using a Nikon Plan-Apochromat ×60 oil-immersion lens (1.4 numerical aperture) with the Nikon C2+ laser scanning confocal microscope. Images were analyzed with NIS-Elements software (Nikon Instruments, Melville, NY) and FIJI/ImageJ (National Institutes of Health, Bethesda, MD) (76, 77).

Wound Closure Assay—Stable MCF-7 cells were seeded in triplicate in a 12-well plate and grown to confluence. A sterile 200-μl tip was used to introduce a scratch-wound in the cell monolayer. The cells were washed once with growth medium to remove cellular debris and replaced with fresh growth medium containing 10% (v/v) FBS. Phase contrast images were captured with a Zeiss AxioCam HRc camera (Carl Zeiss, Thornwood, NY) coupled to the Zeiss Axiovert 200 microscope (×10 objective lens, Carl Zeiss) at 0 and 48 h post-scratch. Relative wound width was measured using ImageJ software (National Institutes of Health).

Statistical Analysis—All experiments were independently replicated two or more times, as indicated in the figure legends. All statistical analysis was performed using Prism version 4 (Graph Pad Software; La Jolla, CA). One-way or two-way analysis of variance (ANOVA) with post hoc Bonferroni's or Tukey's multiple comparison tests were used to analyze differences between groups. Results are typically shown as the mean with error bars representing S.E. *n.s.*, $p > 0.05$; *, $p \leq 0.05$; **, $p \leq 0.01$; ***, $p < 0.001$.

Author Contributions—K. H. designed and performed all of the experiments, analyzed the data, and wrote the manuscript. C. V. C. conceived and supervised the study and wrote the manuscript. All authors reviewed the results and approved the final version of the manuscript.

Acknowledgments—We thank Suzanne Schauwecker from the Clevenger laboratory for insightful discussions of the manuscript. Imaging work was performed at the Northwestern University Center for Advanced Microscopy generously supported by National Institutes of Health Grant CCSG P30 CA06553 from NCI awarded to the Robert H. Lurie Comprehensive Cancer Center.

References

1. Reynolds, C., Montone, K. T., Powell, C. M., Tomaszewski, J. E., and Clevenger, C. V. (1997) Expression of prolactin and its receptor in human breast carcinoma. *Endocrinology* **138,** 5555–5560
2. Meng, J., Tsai-Morris, C. H., and Dufau, M. L. (2004) Human prolactin receptor variants in breast cancer: low ratio of short forms to the long-form human prolactin receptor associated with mammary carcinoma. *Cancer Res.* **64,** 5677–5682
3. Gill, S., Peston, D., Vonderhaar, B. K., and Shousha, S. (2001) Expression of prolactin receptors in normal, benign, and malignant breast tissue: an immunohistological study. *J. Clin. Pathol.* **54,** 956–960

4. DaSilva, L., Howard, O. M., Rui, H., Kirken, R. A., and Farrar, W. L. (1994) Growth signaling and JAK2 association mediated by membrane-proximal cytoplasmic regions of prolactin receptors. *J. Biol. Chem.* **269,** 18267–18270
5. Piazza, T. M., Lu, J. C., Carver, K. C., and Schuler, L. A. (2009) SRC family kinases accelerate prolactin receptor internalization, modulating trafficking and signaling in breast cancer cells. *Mol. Endocrinol.* **23,** 202–212
6. Clevenger, C. V., Furth, P. A., Hankinson, S. E., and Schuler, L. A. (2003) The role of prolactin in mammary carcinoma. *Endocr. Rev.* **24,** 1–27
7. Acosta, J. J., Muñoz, R. M., González, L., Subtil-Rodríguez, A., Dominguez-Caceres, M. A., García-Martínez, J. M., Calcabrini, A., Lazaro-Trueba, I., and Martín-Pérez, J. (2003) Src mediates prolactin-dependent proliferation of T47D and MCF7 cells via the activation of focal adhesion kinase/Erk1/2 and phosphatidylinositol 3-kinase pathways. *Mol. Endocrinol.* **17,** 2268–2282
8. Das, R., and Vonderhaar, B. K. (1996) Involvement of SHC, GRB2, SOS, and RAS in prolactin signal transduction in mammary epithelial cells. *Oncogene* **13,** 1139–1145
9. Das, R., and Vonderhaar, B. K. (1996) Activation of raf-1, MEK, and MAP kinase in prolactin responsive mammary cells. *Breast Cancer Res. Treat.* **40,** 141–149
10. Aksamitiene, E., Achanta, S., Kolch, W., Kholodenko, B. N., Hoek, J. B., and Kiyatkin, A. (2011) Prolactin-stimulated activation of ERK1/2 mitogen-activated protein kinases is controlled by PI3-kinase/Rac/PAK signaling pathway in breast cancer cells. *Cell. Signal.* **23,** 1794–1805
11. Maus, M. V., Reilly, S. C., and Clevenger, C. V. (1999) Prolactin as a chemoattractant for human breast carcinoma. *Endocrinology* **140,** 5447–5450
12. Miller, S. L., Antico, G., Raghunath, P. N., Tomaszewski, J. E., and Clevenger, C. V. (2007) Nek3 kinase regulates prolactin-mediated cytoskeletal reorganization and motility of breast cancer cells. *Oncogene* **26,** 4668–4678
13. Tworoger, S. S., Eliassen, A. H., Zhang, X., Qian, J., Sluss, P. M., Rosner, B. A., and Hankinson, S. E. (2013) A 20-year prospective study of plasma prolactin as a risk marker of breast cancer development. *Cancer Res.* **73,** 4810–4819
14. Tworoger, S. S., and Hankinson, S. E. (2008) Prolactin and breast cancer etiology: an epidemiologic perspective. *J. Mammary Gland Biol. Neoplasia* **13,** 41–53
15. Bhatavdekar, J. M., Shah, N. G., Balar, D. B., Patel, D. D., Bhaduri, A., Trivedi, S. N., Karelia, N. H., Ghosh, N., Shukla, M. K., and Giri, D. D. (1990) Plasma prolactin as an indicator of disease progression in advanced breast cancer. *Cancer* **65,** 2028–2032
16. Mujagić, Z., and Mujagić, H. (2004) Importance of serum prolactin determination in metastatic breast cancer patients. *Croat Med. J.* **45,** 176–180
17. Yonezawa, T., Chen, K. H., Ghosh, M. K., Rivera, L., Dill, R., Ma, L., Villa, P. A., Kawaminami, M., and Walker, A. M. (2015) Anti-metastatic outcome of isoform-specific prolactin receptor targeting in breast cancer. *Cancer Lett.* **366,** 84–92
18. Schultz, S. J., Fry, A. M., Sütterlin, C., Ried, T., and Nigg, E. A. (1994) Cell cycle-dependent expression of Nek2, a novel human protein kinase related to the NIMA mitotic regulator of *Aspergillus nidulans*. *Cell Growth Differ.* **5,** 625–635
19. Schultz, S. J., and Nigg, E. A. (1993) Identification of 21 novel human protein kinases, including 3 members of a family related to the cell cycle regulator nimA of *Aspergillus nidulans*. *Cell Growth Differ.* **4,** 821–830
20. Hashimoto, Y., Akita, H., Hibino, M., Kohri, K., and Nakanishi, M. (2002) Identification and characterization of Nek6 protein kinase, a potential human homolog of NIMA histone H3 kinase. *Biochem. Biophys. Res. Commun.* **293,** 753–758
21. Rogers, S., Wells, R., and Rechsteiner, M. (1986) Amino acid sequences common to rapidly degraded proteins: the PEST hypothesis. *Science* **234,** 364–368
22. Ridley, A. J., Schwartz, M. A., Burridge, K., Firtel, R. A., Ginsberg, M. H., Borisy, G., Parsons, J. T., and Horwitz, A. R. (2003) Cell migration: integrating signals from front to back. *Science* **302,** 1704–1709
23. Etienne-Manneville, S., and Hall, A. (2002) Rho GTPases in cell biology. *Nature* **420,** 629–635
24. Miller, S. L., DeMaria, J. E., Freier, D. O., Riegel, A. M., and Clevenger, C. V. (2005) Novel association of Vav2 and Nek3 modulates signaling through the human prolactin receptor. *Mol. Endocrinol.* **19,** 939–949
25. Fry, A. M., Schultz, S. J., Bartek, J., and Nigg, E. A. (1995) Substrate specificity and cell cycle regulation of the Nek2 protein kinase, a potential human homolog of the mitotic regulator NIMA of *Aspergillus nidulans*. *J. Biol. Chem.* **270,** 12899–12905
26. Rellos, P., Ivins, F. J., Baxter, J. E., Pike, A., Nott, T. J., Parkinson, D. M., Das, S., Howell, S., Fedorov, O., Shen, Q. Y., Fry, A. M., Knapp, S., and Smerdon, S. J. (2007) Structure and regulation of the human Nek2 centrosomal kinase. *J. Biol. Chem.* **282,** 6833–6842
27. Bertran, M. T., Sdelci, S., Regué, L., Avruch, J., Caelles, C., and Roig, J. (2011) Nek9 is a Plk1-activated kinase that controls early centrosome separation through Nek6/7 and Eg5. *EMBO J.* **30,** 2634–2647
28. Roig, J., Groen, A., Caldwell, J., and Avruch, J. (2005) Active Nercc1 protein kinase concentrates at centrosomes early in mitosis and is necessary for proper spindle assembly. *Mol. Biol. Cell* **16,** 4827–4840
29. Tanaka, K., and Nigg, E. A. (1999) Cloning and characterization of the murine Nek3 protein kinase, a novel member of the NIMA family of putative cell cycle regulators. *J. Biol. Chem.* **274,** 13491–13497
30. Chang, J., Baloh, R. H., and Milbrandt, J. (2009) The NIMA-family kinase Nek3 regulates microtubule acetylation in neurons. *J. Cell Sci.* **122,** 2274–2282
31. Zalli, D., Bayliss, R., and Fry, A. M. (2012) The Nek8 protein kinase, mutated in the human cystic kidney disease nephronophthisis, is both activated and degraded during ciliogenesis. *Hum. Mol. Genet.* **21,** 1155–1171
32. Liu, S., Ho, C. K., Ouyang, J., and Zou, L. (2013) Nek1 kinase associates with ATR-ATRIP and primes ATR for efficient DNA damage signaling. *Proc. Natl. Acad. Sci. U.S.A.* **110,** 2175–2180
33. Nolen, B., Taylor, S., and Ghosh, G. (2004) Regulation of protein kinases; controlling activity through activation segment conformation. *Mol. Cell* **15,** 661–675
34. Bayliss, R., Fry, A., Haq, T., and Yeoh, S. (2012) On the molecular mechanisms of mitotic kinase activation. *Open Biol.* **2,** 120136
35. Belham, C., Roig, J., Caldwell, J. A., Aoyama, Y., Kemp, B. E., Comb, M., and Avruch, J. (2003) A mitotic cascade of NIMA family kinases. Nercc1/Nek9 activates the Nek6 and Nek7 kinases. *J. Biol. Chem.* **278,** 34897–34909
36. Eyers, P. A., and Maller, J. L. (2004) Regulation of *Xenopus* Aurora A activation by TPX2. **279,** 9008–9015
37. Anthis, N. J., Haling, J. R., Oxley, C. L., Memo, M., Wegener, K. L., Lim, C. J., Ginsberg, M. H., and Campbell, I. D. (2009) β integrin tyrosine phosphorylation is a conserved mechanism for regulating talin-induced integrin activation. *J. Biol. Chem.* **284,** 36700–36710
38. Obenauer, J. C., Cantley, L. C., and Yaffe, M. B. (2003) Scansite 2.0: Proteome-wide prediction of cell signaling interactions using short sequence motifs. *Nucleic Acids Res.* **31,** 3635–3641
39. Gonzalez, F. A., Raden, D. L., and Davis, R. J. (1991) Identification of substrate recognition determinants for human ERK1 and ERK2 protein kinases. *J. Biol. Chem.* **266,** 22159–22163
40. Payne, D. M., Rossomando, A. J., Martino, P., Erickson, A. K., Her, J. H., Shabanowitz, J., Hunt, D. F., Weber, M. J., and Sturgill, T. W. (1991) Identification of the regulatory phosphorylation sites in pp42/mitogen-activated protein kinase (MAP kinase). *EMBO J.* **10,** 885–892
41. Caunt, C. J., Sale, M. J., Smith, P. D., and Cook, S. J. (2015) MEK1 and MEK2 inhibitors and cancer therapy: the long and winding road. *Nat. Rev. Cancer* **15,** 577–592
42. Shaul, Y. D., and Seger, R. (2007) The MEK/ERK cascade: from signaling specificity to diverse functions. *Biochim. Biophys. Acta* **1773,** 1213–1226
43. Llovera, M., Pichard, C., Bernichtein, S., Jeay, S., Touraine, P., Kelly, P. A., and Goffin, V. (2000) Human prolactin (hPRL) antagonists inhibit hPRL-activated signaling pathways involved in breast cancer cell proliferation. *Oncogene* **19,** 4695–4705
44. Bole-Feysot, C., Goffin, V., Edery, M., Binart, N., and Kelly, P. A. (1998) Prolactin (PRL) and its receptor: actions, signal transduction pathways and phenotypes observed in PRL receptor knockout mice. *Endocr. Rev.* **19,** 225–268

45. Barcus, C. E., Keely, P. J., Eliceiri, K. W., and Schuler, L. A. (2013) Stiff collagen matrices increase tumorigenic prolactin signaling in breast cancer cells. *J. Biol. Chem.* **288,** 12722–12732
46. Kamakura, S., Moriguchi, T., and Nishida, E. (1999) Activation of the protein kinase ERK5/BMK1 by receptor tyrosine kinases. Identification and characterization of a signaling pathway to the nucleus. *J. Biol. Chem.* **274,** 26563–26571
47. Mody, N., Leitch, J., Armstrong, C., Dixon, J., and Cohen, P. (2001) Effects of MAP kinase cascade inhibitors on the MKK5/ERK5 pathway. *FEBS Lett.* **502,** 21–24
48. Gutzman, J. H., Rugowski, D. E., Schroeder, M. D., Watters, J. J., and Schuler, L. A. (2004) Multiple kinase cascades mediate prolactin signals to activating protein-1 in breast cancer cells. *Mol. Endocrinol.* **18,** 3064–3075
49. Pullikuth, A. K., and Catling, A. D. (2010) Extracellular signal-regulated kinase promotes Rho-dependent focal adhesion formation by suppressing p190A RhoGAP. *Mol. Cell. Biol.* **30,** 3233–3248
50. Webb, D. J., Donais, K., Whitmore, L. A., Thomas, S. M., Turner, C. E., Parsons, J. T., and Horwitz, A. F. (2004) FAK-Src signalling through paxillin, ERK and MLCK regulates adhesion disassembly. *Nat. Cell Biol.* **6,** 154–161
51. Vomastek, T., Iwanicki, M. P., Schaeffer, H. J., Tarcsafalvi, A., Parsons, J. T., and Weber, M. J. (2007) RACK1 targets the extracellular signal-regulated kinase/mitogen-activated protein kinase pathway to link integrin engagement with focal adhesion disassembly and cell motility. *Mol. Cell. Biol.* **27,** 8296–8305
52. Nobes, C. D., and Hall, A. (1999) Rho GTPases control polarity, protrusion, and adhesion during cell movement. *J. Cell Biol.* **144,** 1235–1244
53. Webb, D. J., Parsons, J. T., and Horwitz, A. F. (2002) Adhesion assembly, disassembly and turnover in migrating cells–over and over and over again. *Nat. Cell Biol.* **4,** E97–E100
54. Zaidel-Bar, R., Ballestrem, C., Kam, Z., and Geiger, B. (2003) Early molecular events in the assembly of matrix adhesions at the leading edge of migrating cells. *J. Cell Sci.* **116,** 4605–4613
55. Lu, K. P., Kemp, B. E., and Means, A. R. (1994) Identification of substrate specificity determinants for the cell cycle-regulated NIMA protein kinase. *J. Biol. Chem.* **269,** 6603–6607
56. Huang, C., Jacobson, K., and Schaller, M. D. (2004) MAP kinases and cell migration. *J. Cell Sci.* **117,** 4619–4628
57. Ono, H., Basson, M. D., and Ito, H. (2014) PTK6 promotes cancer migration and invasion in pancreatic cancer cells dependent on ERK signaling. *PLoS One* **9,** e96060
58. Klemke, R. L., Cai, S., Giannini, A. L., Gallagher, P. J., de Lanerolle, P., and Cheresh, D. A. (1997) Regulation of cell motility by mitogen-activated protein kinase. *J. Cell Biol.* **137,** 481–492
59. Fincham, V. J., James, M., Frame, M. C., and Winder, S. J. (2000) Active ERK/MAP kinase is targeted to newly forming cell-matrix adhesions by integrin engagement and v-Src. *EMBO J.* **19,** 2911–2923
60. Chen, H., Zhu, G., Li, Y., Padia, R. N., Dong, Z., Pan, Z. K., Liu, K., and Huang, S. (2009) Extracellular signal-regulated kinase signaling pathway regulates breast cancer cell migration by maintaining slug expression. *Cancer Res.* **69,** 9228–9235
61. Lester, R. D., Jo, M., Campana, W. M., and Gonias, S. L. (2005) Erythropoietin promotes MCF-7 breast cancer cell migration by an ERK/mitogen-activated protein kinase-dependent pathway and is primarily responsible for the increase in migration observed in hypoxia. *J. Biol. Chem.* **280,** 39273–39277
62. Zaidel-Bar, R., and Geiger, B. (2010) The switchable integrin adhesome. *J. Cell Sci.* **123,** 1385–1388
63. Costa, P., Scales, T. M., Ivaska, J., and Parsons, M. (2013) Integrin-specific control of focal adhesion kinase and RhoA regulates membrane protrusion and invasion. *PLoS One* **8,** e74659
64. Galbaugh, T., Feeney, Y. B., and Clevenger, C. V. (2010) Prolactin receptor-integrin cross-talk mediated by SIRPα in breast cancer cells. *Mol. Cancer Res.* **8,** 1413–1424
65. Fagerholm, S. C., Hilden, T. J., and Gahmberg, C. G. (2004) P marks the spot: site-specific integrin phosphorylation regulates molecular interactions. *Trends Biochem. Sci.* **29,** 504–512
66. Li, Z., Zhang, H., Lundin, L., Thullberg, M., Liu, Y., Wang, Y., Claesson-Welsh, L., and Strömblad, S. (2010) p21-activated kinase 4 phosphorylation of integrin beta5 Ser-759 and Ser-762 regulates cell migration. *J. Biol. Chem.* **285,** 23699–23710
67. Nayal, A., Webb, D. J., Brown, C. M., Schaefer, E. M., Vicente-Manzanares, M., and Horwitz, A. R. (2006) Paxillin phosphorylation at Ser273 localizes a GIT1-PIX-PAK complex and regulates adhesion and protrusion dynamics. *J. Cell Biol.* **173,** 587–589
68. Parsons, J. T., Horwitz, A. R., and Schwartz, M. A. (2010) Cell adhesion: integrating cytoskeletal dynamics and cellular tension. *Nat. Rev. Mol. Cell Biol.* **11,** 633–643
69. Burridge, K., and Wennerberg, K. (2004) Rho and Rac take center stage. *Cell* **116,** 167–179
70. Guilluy, C., Garcia-Mata, R., and Burridge, K. (2011) Rho protein crosstalk: another social network? *Trends Cell Biol.* **21,** 718–726
71. Pertz, O. (2010) Spatio-temporal Rho GTPase signaling–where are we now? *J. Cell Sci.* **123,** 1841–1850
72. Brunet, A., Pagès, G., and Pouysségur, J. (1994) Constitutively active mutants of MAP kinase kinase (MEK1) induce growth factor-relaxation and oncogenicity when expressed in fibroblasts. *Oncogene* **9,** 3379–3387
73. Scholl, F. A., Dumesic, P. A., and Khavari, P. A. (2004) Mek1 alters epidermal growth and differentiation. *Cancer Res.* **64,** 6035–6040
74. Campeau, E., Ruhl, V. E., Rodier, F., Smith, C. L., Rahmberg, B. L., Fuss, J. O., Campisi, J., Yaswen, P., Cooper, P. K., and Kaufman, P. D. (2009) A versatile viral system for expression and depletion of proteins in mammalian cells. *PloS one* **4,** e6529
75. Tong, J., Li, L., Ballermann, B., and Wang, Z. (2013) Phosphorylation of Rac1 T108 by extracellular signal-regulated kinase in response to epidermal growth factor: a novel mechanism to regulate Rac1 function. *Mol. Cell. Biol.* **33,** 4538–4551
76. Schindelin, J., Arganda-Carreras, I., Frise, E., Kaynig, V., Longair, M., Pietzsch, T., Preibisch, S., Rueden, C., Saalfeld, S., Schmid, B., Tinevez, J. Y., White, D. J., Hartenstein, V., Eliceiri, K., Tomancak, P., and Cardona, A. (2012) Fiji: an open-source platform for biological-image analysis. *Nat. Methods* **9,** 676–682
77. Schneider, C. A., Rasband, W. S., and Eliceiri, K. W. (2012) NIH Image to ImageJ: 25 years of image analysis. *Nat. Methods* **9,** 671–675